

Inelastic Kapitza-Dirac scattering: A scalable tool for deterministic preparation of non-Gaussian oscillator states

Wayne Cheng-Wei Huang,^{1,*} Herman Batelaan,² and Markus Arndt³

¹*Department of Physics and Astronomy, Northwestern University, Evanston, Illinois 60208, USA*

²*Department of Physics and Astronomy, University of Nebraska-Lincoln, Lincoln, Nebraska 68588, USA*

³*Faculty of Physics, University of Vienna, Boltzmannngasse 5, A-1090 Vienna, Austria*

Harmonic oscillators count among the most fundamental quantum systems with important applications in quantum optics, solid-state physics, molecular physics, nanoparticle trapping, and quantum information processing. They are distinguished by their equidistant energy level spacing, a feature that is often desired but also a challenge if the goal is to deterministically populate specific target states. Here, we propose to use the *inelastic* Kapitza-Dirac effect as a means to solve this challenge. Quantum interference in inelastic Kapitza-Dirac scattering can suppress the sequential climbing of harmonic oscillator states and achieve selective excitation to Schrödinger cat states or other non-Gaussian states for a wide range of harmonically trapped particles. We discuss the feasibility of experiments with single electrons, complex molecules, and dielectric nanoparticles.

The harmonic oscillator is a paradigmatic text book example of fundamental quantum physics and it has remained at the heart of modern research. Quantum harmonic oscillators have been realized with single electrons [1, 2], single ions [3], ultracold quantum gases [4], and dielectric nanoparticles [5]. For all these systems, cooling to the oscillator ground state has been successfully demonstrated. Our present proposal is motivated by the challenge to prepare highly non-classical states, such as mesoscopic Schrödinger cat states, independent of the detailed properties of the oscillator.

Schrödinger's thought experiment illustrates the possibility of a macroscopic body being in a quantum superposition of two states that would be classically mutually exclusive [6]. Throughout the last two decades, macroscopic quantum superposition has been addressed by several experiments for widely different systems [7]. Neutrons were delocalized over 10 cm [8]. Atoms were put in superpositions on the half-meter scale [9] and in distinct momentum states separated by more than 1000 $\hbar k$ [10]. Large organic molecules exceeding 25,000 Da have been delocalized over hundreds of nanometers [11]. Moreover, it is proposed to prepare massive dielectric nanoparticles in distinct position states [7, 12] to test the nature of quantum collapse [13], quantum decoherence [14–16], or the quantum nature of gravity [17, 18].

Here we propose to exploit *inelastic* Kapitza-Dirac (KD) scattering in a harmonic trap as a universal tool for preparing Schrödinger cat states, or non-Gaussian states in general, for particles as different as single electrons, complex molecules, and dielectric nanoparticles, differing in mass by more than nine orders of magnitude.

In the original proposal by Kapitza and Dirac [19], electrons were assumed to be coherently scattered by the

pondermotive force of a standing light wave. It took several advances in electron beam and laser technology to realize this idea 70 years later, both in the Raman-Nath and in the Bragg regime [20, 21]. In parallel, the idea of optical phase gratings has also been extended to atoms [22–24], and even complex molecules [25, 26], where the interaction is mediated by the optical dipole force between the laser electric field and the polarizability of the massive particle.

The *inelastic* KD effect differs from its *elastic* counterpart by the presence of laser fields with different frequencies and a 1D harmonic trap (see FIG. 1) [27]. The latter helps conserve energy and momentum. We start for simplicity with the example of a free electron passing through a 1D trap.

A 1D electron trap can be realized by the pondermotive potential of a standing light wave [28, 29]. Optical trapping for electrons is an effective way for reaching high trap frequency as well as avoiding thermal and

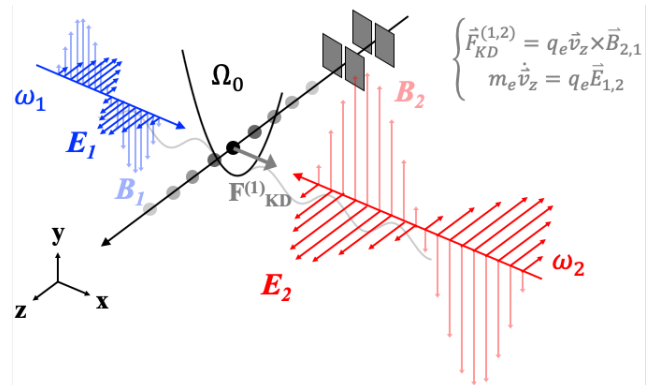


FIG. 1. (color online) Proposed experimental scheme for electrons. Two counter-propagating KD lasers of frequencies ω_1 and ω_2 (blue and red) interact with the electron in the 1D harmonic trap. The difference of the KD laser frequencies leads to unbalanced Lorentz forces $F_{\text{KD}}^{(1,2)}$ (top-right).

* Email: waynehuang1984@gmail.com

Current address: University of Göttingen, IV. Physical Institute – Solids and Nanostructures, 370077 Göttingen, Germany.

electric excitation by nearby walls and electrodes. We consider a standing wave in the x -direction with a polarization along the y -axis. Close to the potential minimum $x_m = \lambda_{\text{TL}}/4$, where λ_{TL} is the trapping laser wavelength, the potential can be approximated as a harmonic trap $U_p(x) \approx (q_e^2 I_s / 2\epsilon_0 c^3 m_e) x^2$, where m_e and q_e are the electron mass and charge, and I_s is the standing wave intensity. The pondermotive trap frequency is

$$\Omega_0 = \sqrt{\frac{q_e^2 I_s}{\epsilon_0 c^3 m_e}}. \quad (1)$$

The trapping laser intensity is $I_{\text{TL}} = I_s/4$. We assume that the ground state of the harmonic trap is fully populated by a well-collimated electron beam with a transverse kinetic energy $mv_x^2/2 \ll \hbar\Omega_0/2$.

Two KD lasers with frequencies $\omega_{1,2}$ ($\omega_1 > \omega_2$) counter-propagate along the x -axis and interact with the electron while it is in the 1D trap (see FIG. 1). The polarizations of the KD lasers are along the z -axis to avoid undesired high-order elastic KD scattering via wave mixing with the trapping laser [30–32]. Interacting with both KD laser fields, the electron experiences a net force in the x -direction at the difference frequency [27, 28]. The effective KD potential is

$$V_{\text{KD}}(\hat{x}, t) = \frac{q_e^2 A^2(t)}{2m_e} \cos((k_1 + k_2)\hat{x}) \cos((\omega_1 - \omega_2)t), \quad (2)$$

where $A^2(t) \equiv A_1 A_2 \exp(-2t^2/\tau_{\text{KD}}^2)$, $A_{1,2}$ are the vector potential amplitudes of the KD lasers, and τ_{KD} is the pulse duration. If $\omega_1 - \omega_2$ is chosen to be a multiple of Ω_0 , the electron oscillator can be parametrically driven [27, 28, 33]. Specifically, the parametric resonance occurs when the energy-momentum conservations are satisfied,

$$\begin{cases} \omega_1 - \omega_2 = n_e \Omega_0 \\ k_1 + k_2 = (n_e + \delta_p) k_0, \end{cases} \quad (3)$$

where n_e is a positive integer and $\delta_p \geq -n_e$. The parameter δ_p is dimensionless and it characterizes the detuning from the maximum momentum transfer $n_e \hbar k_0$. We interpret $n_e \hbar k_0$ as the maximum momentum transfer because the overlap between the initial and final momentum wavefunctions starts to decrease when the momentum transfer $\hbar(k_1 + k_2)$ exceeds $n_e \hbar k_0$, where $\hbar k_0 = \sqrt{\hbar m_e \Omega_0/2}$ is the standard deviation of the oscillator's ground-state momentum probability distribution. We define δ_p as the momentum detuning hereafter.

The resonant KD laser frequencies ω_1 and ω_2 can be found through Eq. (3), $\omega_{1,2} = \omega_{\text{KD}} \pm n_e \Omega_0/2$, where the central KD laser frequency is

$$\omega_{\text{KD}} \equiv (n_e + \delta_p) c k_0/2. \quad (4)$$

Here we remark that *inelastic* KD scattering and stimulated Raman scattering [34–37] are similar in that they

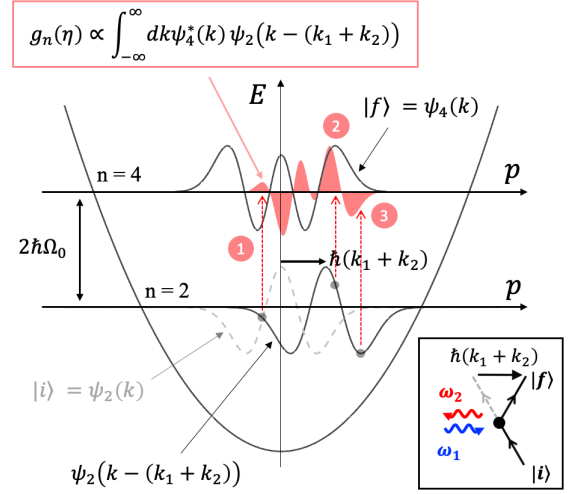


FIG. 2. (color online) Kapitza-Dirac blockade. An electron in the state $|n=2\rangle$ makes a transition to $|n=4\rangle$ after receiving a momentum recoil $\hbar(k_1 + k_2)$ and energy $\hbar(\omega_1 - \omega_2) = 2\hbar\Omega_0$ from stimulated absorption (inset). The dashed red arrows illustrate three transition paths from $|n=2\rangle$ to $|n=4\rangle$. The KD blockade occurs when the sum of all transition amplitudes (red bumps) is zero, i.e. complete destructive interference.

both produce a large momentum transfer $\hbar(k_1 + k_2)$ with a small energy exchange $\hbar(\omega_1 - \omega_2)$. However, in contrast to stimulated Raman scattering, *inelastic* KD scattering does not involve any intermediate quantum states, so the KD laser frequency can be far detuned from electronic transitions and mitigate problems associated with spontaneous emission [38].

To demonstrate the preparation of non-Gaussian states, we first evaluate the dimensionless transition amplitude $g_n(\eta) = \langle n+2 | \cos((k_1 + k_2)\hat{x}) | n \rangle$ in the Schrödinger equation that corresponds to the case of $n_e = 2$ [28, 39, 40],

$$g_n(\eta) = -\sqrt{\frac{n!}{(n+2)!}} \eta^2 L_n^{(2)}(\eta^2) e^{-\eta^2/2}, \quad (5)$$

where $L_n^{(2)}(y)$ is the generalized Laguerre polynomial. The Lamb-Dicke parameter is defined as $\eta \equiv (k_1 + k_2)x_0$, where $x_0 = \sqrt{\hbar/2m_e\Omega_0}$ is the standard deviation of the oscillator's ground-state position probability distribution. The transition amplitude $g_n(\eta)$ has zero-crossings, which imply that the transition $|n\rangle \rightarrow |n+2\rangle$ can be fully suppressed at certain values of the momentum detuning δ_p . The suppression occurs because of destructive interference among different transition paths as illustrated in FIG. 2. We call this interference effect the *Kapitza-Dirac blockade*, and we will exploit it to stop sequential excitation in order to prepare non-Gaussian states. We remark that Eq. (3) implies that the Lamb-Dicke parameter in Eq. (5) is a generic quantity, $\eta = (n_e + \delta_p)/2$, independent of all oscillator properties. Therefore, the momentum de-

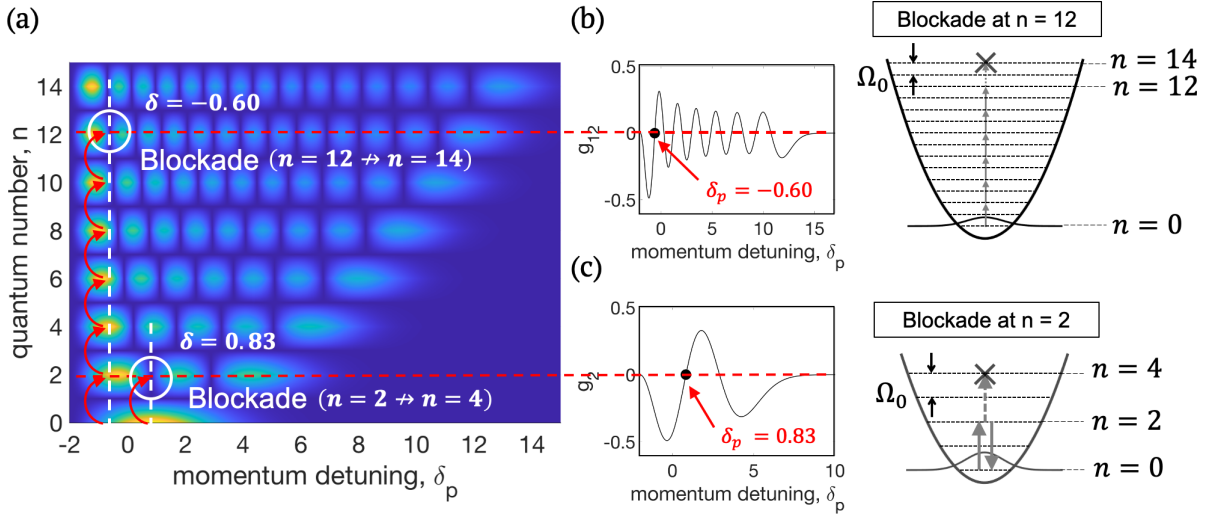


FIG. 3. (color online) Transition map for the *inelastic* Kapitza-Dirac effect. (a) The norm of the transition amplitude $|g_n|$ in Eq. (5) is plotted as a function of the quantum number n and the momentum detuning δ_p . The nodes along the δ_p -axis (white circles) can be used to stop sequential excitations (red curved arrows). (b) The zero-crossing of $g_{12}(\eta)$ at $\delta_p = -0.60$ is used to stop transitions beyond $|n = 12\rangle$. (c) The zero-crossing $g_2(\eta)$ at $\delta_p = 0.83$ is used to prepare an effective two-level system between $|n = 0\rangle$ and $|n = 2\rangle$.

tuning δ_p required for a KD blockade is universal and the same for all oscillators.

As the first example, we will use KD blockade to prepare a ground-state electron oscillator in a single eigenstate $|n = 2\rangle$. We start by setting $\delta_p = 0.83$, which suppresses the $|n = 2\rangle \rightarrow |n = 4\rangle$ transition down to 0.2% of its maximum value. As a result, transitions can only be driven between $|n = 0\rangle$ and $|n = 2\rangle$ (see FIG. 3). The Rabi frequency for this effective two-level system is obtained from the Schrödinger equation, $\Omega_R = (q_e^2 A_1 A_2 / 2m_e \hbar) |g_0(\eta)|$. For a Gaussian-shaped time envelope, population inversion, i.e. a π -pulse, can be obtained for

$$\Omega_R \left(\sqrt{\frac{\pi}{2}} \tau_{\text{KD}} \right) = \pi. \quad (6)$$

Using $\tau_{\text{KD}} = \sqrt{2\pi}/\Omega_R$, all population in $|n = 0\rangle$ can be transferred to $|n = 2\rangle$ as shown in FIG. 4(a). Note that τ_{KD} should be sufficiently long to keep the pulse bandwidth below the trap frequency Ω_0 and avoid off-resonant excitation. When the pulse duration is doubled, the Rabi cycle is completed and all population is coherently driven back to the ground state (see FIG. 4(b)). This shows how KD blockade can transform a harmonic oscillator with many equally spaced energy levels into an effective two-level system, thus realizing a novel element for quantum information processing.

As a second example, we will use the KD blockade to prepare a Schrödinger cat state. We set the momentum detuning $\delta_p = -0.60$ to suppress the transition $|n = 12\rangle \rightarrow |n = 14\rangle$ down to 0.1% of its maximum value. The electron oscillator undergoes a sequential ex-

citation from $|n = 0\rangle$, at steps of $\Delta n = 2$, and stops at $|n = 12\rangle$ (see FIG. 3). The pulse intensity I_{KD} and the pulse duration τ_{KD} are adjusted together to position the peak of the population distribution at $n_{\text{max}} = 8$ with a width narrower than that of a Poisson distribution while avoiding off-resonant excitation (see FIG. 4(c)). Such a sub-Poissonian width is a feature of the KD blockade, and it leads to an amplitude-squeezed Schrödinger cat state as illustrated by the electron's Wigner function shown in FIG. 4(d) [28]. The maximum spatial and momentum separation of the cat state, Δx_{cat} and Δp_{cat} , are [28]

$$\frac{\Delta x_{\text{cat}}}{x_0} = \frac{\Delta p_{\text{cat}}}{\hbar k_0} \approx 4\sqrt{n_{\text{max}}}. \quad (7)$$

Substituting Eq. (3) to Eq. (7) with $n_e = 2$, the number of photon recoils is

$$N_{\text{ph}} = \frac{\Delta p_{\text{cat}}}{\hbar(k_1 + k_2)} \approx \frac{4\sqrt{n_{\text{max}}}}{2 + \delta_p}, \quad (8)$$

which is again independent of the oscillator's properties. If we take $n_{\text{max}} = 650$ and $\delta_p = -1.8$, the maximum momentum separation is $\Delta p_{\text{cat}} \approx 1000 \hbar k$, where $k = 2\pi/532\text{nm}$. Assuming that the electron oscillator reaches the maximum momentum separation as the electron leaves the trap (see FIG. 1), there will be two distinct wavepackets separated by $270 \mu\text{m}$ in real space at 1 mm after the trap, which makes a wide-angle coherent beamsplitter [41–43]. Therefore, *inelastic* KD scattering shows promise for an unprecedented all-optical large-momentum-transfer (LMT) beamsplitter [9, 10, 44, 45]. Additionally, the narrowed momentum width of the amplitude-squeezed Schrödinger cat state

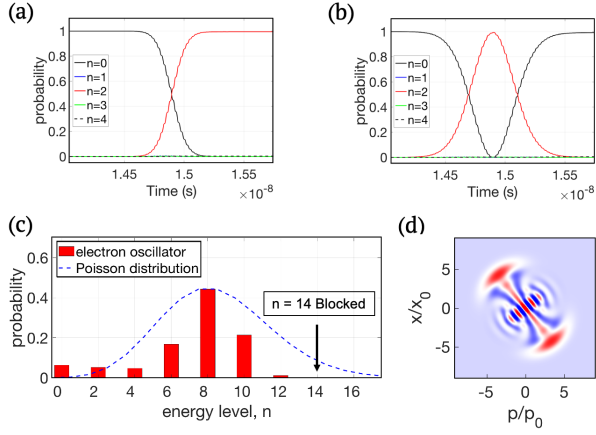


FIG. 4. (color online) Single eigenstates and Schrödinger cat states of electron. (a) Full population transfer to the $|n=2\rangle$ eigenstate can be achieved with $\lambda_{\text{KD}} = 263$ nm and a π -pulse. (b) When the KD pulse duration in (a) is doubled, the population is coherently brought back to the ground state. (c) The population distribution of a Schrödinger cat state prepared by $\lambda_{\text{KD}} = 532$ nm has a standard deviation less than the Poissonian width $\sigma_p = \sqrt{n_{\text{max}}}$. (d) The Wigner function of the cat state indicates amplitude squeezing. Note that $p_0 \equiv \hbar k_0$.

makes the split beam well-collimated. A KD-LMT beam-splitter used in conjunction with an optical Bragg grating [20, 46] can facilitate high-resolution, large-area matter-wave interferometry.

Other non-Gaussian states such as multi-component cat states [47–49] can be prepared by properly chosen n_e and δ_p . An example is given in FIG. 5 where a 3-component cat state is prepared. The KD laser frequencies $\omega_{1,2}$ in this case are determined by taking $n_e = 3$ and $\delta_p = -1.57$, which suppresses the transition $|n=18\rangle \rightarrow |n=21\rangle$ [28]. Similar to multi-slit diffraction, interference among all three components of the cat state produces sharper fringes compared to those between each pair. Thus, a multi-component cat state can be a more sensitive probe to quantum decoherence or collapse effects. We also note that Gaussian states can be prepared by taking $n_e = 2$ (vacuum squeezed state) or $n_e = 1$ (displaced squeezed or coherent states) with appropriate I_{KD} and δ_p .

Next, we discuss possible experimental implementations of *inelastic* KD scattering for complex molecules and dielectric nanoparticles. Here, we choose functionalized porphyrins TPPF84 for their high mass, moderate polarizability, and ease to evaporate [50]. For the nanoparticle material, we choose silicon dioxide (SiO_2) because its absorption coefficient is low in the infrared spectrum. The proposed experimental schemes for both particles are similar to FIG. 1 except that the trapping laser is a running wave along the y -axis. The vertical orientation allows trapping for molecules and nanoparticles along the x -axis through the gradient force [28]. With

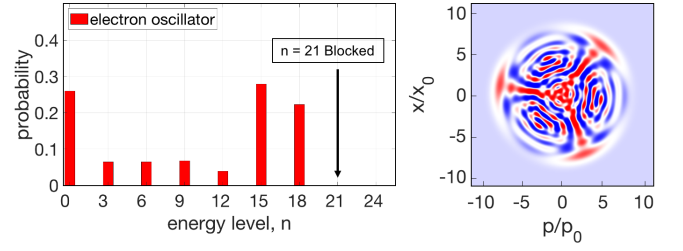


FIG. 5. (color online) Multi-component Schrödinger cat states. Left: A population distribution for a 3-component cat state can be prepared by taking $n_e = 3$ and $\delta_p = -1.57$ in Eq. (3). Right: the Wigner function of the 3-component cat state shows interference fringes between each pair and among all three components.

$W_{x\text{-TL}}$ as the $1/e$ beam diameter along the x -axis, the dipole trap frequency is

$$\Omega_0 = \sqrt{\frac{8\alpha I_{\text{TL}}}{\epsilon_0 c M W_{x\text{-TL}}^2}}, \quad (9)$$

where α and M are the particle's polarizability and mass. Again, we assume that the particle beam is well-collimated or sufficiently cooled so that the ground state of the harmonic trap is fully populated.

There are three criteria for choosing experimental parameters. First, the laser conditions should satisfy the relation $\tau_{\text{TL}} \gg W_{z\text{-TL}}/2v_z \gg W_{z\text{-KD}}/2v_z \gg \tau_{\text{KD}} \gg 2\pi/\Omega_0$ [28], where τ is the $1/e$ pulse duration, W_z is the $1/e$ beam diameter along the z -axis, and v_z is the particle speed in the z -direction. The subscripts -TL and -KD denote the trapping and the KD lasers respectively. Second, the number of elastically scattered ¹ photons n_{sca} should be less than 1 to avoid decoherence and dephasing. Third, the central KD frequency ω_{KD} should be in the visible or the infrared regime because ultraviolet light gets absorbed strongly in materials. This implies that low trap frequencies are preferred for massive particles. The proposed experimental parameters for preparing large amplitude-squeezed Schrödinger cat states for electrons, molecules (TPPF84), and nanoparticles (SiO_2) are listed in Table I. While there are many possible choices for parameters, the proposed parameters are designed to achieve large momentum transfers that surpass state-of-the-art matter-wave beamsplitters [9, 10, 26, 44, 45]. The simulation results for the proposed parameters are summarized in FIG. 6. The simulations were performed on a supercomputer using time-dependent Schrödinger equations [33]. In FIG. 6, the maximum momentum separations Δp_{cat} for electrons and

¹ It is Thomson scattering for electrons and Rayleigh scattering for molecules and nanoparticles.

TABLE I. Proposed experimental parameters for preparing large amplitude-squeezed Schrödinger cat states. The trapping laser for electrons has a $1/e$ pulse duration of $\tau_{\text{TL}} = 0.75$ ns and a repetition rate of 10 Hz. The momentum detunings for electron, molecule (TPPF84), and nanoparticle (SiO_2) are $\delta_p = -1.8$, -1.94 , and -1.95 respectively.

parameters	electron	TPPF84	SiO_2 nanoparticle
M (u)	5.49×10^{-4}	2.81×10^3	10^6
α (Cm^2/V)	-	2.22×10^{-38}	8.18×10^{-36}
Ω_0 (rad/s)	3.2×10^{12}	1.3×10^5	1.75×10^3
λ_{TL} (nm)	1064	10500	10500
$W_{x\text{-TL}}$ (μm)	-	3	6.5
$W_{y\text{-TL}}$ (mm)	0.1	-	-
$W_{z\text{-TL}}$ (mm)	4	2	9
$\langle P_{\text{TL}} \rangle$ (W)	94	50	0.4
v_z (m/s)	5×10^6	0.1	0.1
λ_{KD} (nm)	533	4039	2116
$W_{y\text{-KD}}$ (mm)	0.1	0.01	1
$W_{z\text{-KD}}$ (mm)	1	0.4	8
$\langle P_{\text{KD}} \rangle$ (W)	0.330	1.19	0.126
τ_{KD} (s)	2×10^{-11}	5×10^{-4}	3.5×10^{-2}
n_{sca}	1.7×10^{-10}	1×10^{-3}	0.53

molecules exceed $1000 \hbar k$ and $600 \hbar k$, respectively². The maximum spatial separation for the nanoparticle in the trap is more than 400 nm. If 2D or 3D harmonic traps are used, there can also be entanglement among different motional degrees of freedom [28].

In conclusion, we propose to use the *inelastic* Kapitza-Dirac effect for manipulating the motional quantum states of single electrons, complex molecules, and dielectric nanoparticles. The excitation scheme is universally applicable for very different particles and independent of trap details and dimensions. We demonstrate through simulations the experimental feasibility of preparing various non-Gaussian states for electrons, and amplitude-squeezed Schrödinger cat states for all three particles. The latter has applications for all-optical LMT beam splitters in (high-mass) matter-wave interferometry. The proposed control scheme can also be employed for ions and neutral atoms in 3D harmonic traps without invoking the internal states, which can complement the existing methods in quantum computing and quantum simulation.

The authors thank Aephraim M. Steinberg, Peter W. Milonni, Christopher Monroes, and Uroš Delić for advice and discussions. W. C. Huang wishes to give a special thanks to Yanshuo Li for supports and helpful discussions. This work utilized high-performance computing

² The highest eigenstate attainable is determined by the validity range of the harmonic approximation for the trap [28].

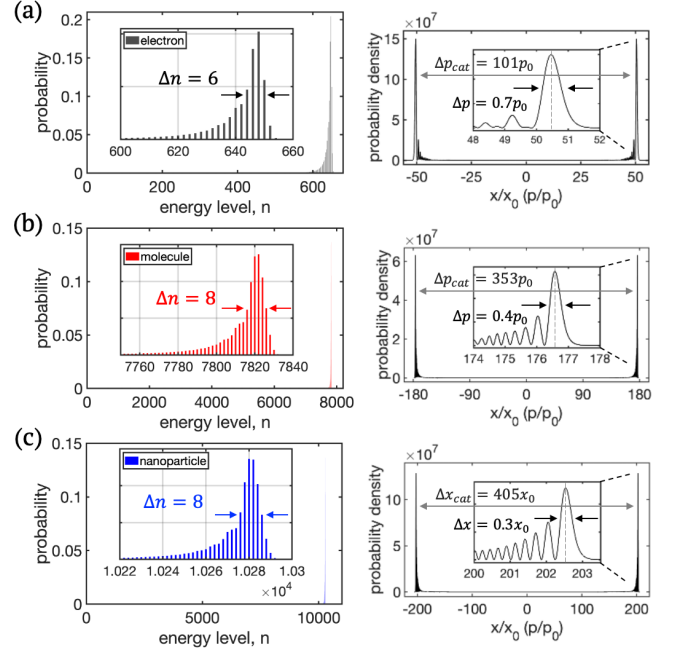


FIG. 6. (color online) Simulation results for parameters in Table I. The maximum momentum separations of the electron (a) and the molecule (b) exceed $1000 \hbar k$ and $600 \hbar k$, where $k = 2\pi/532\text{nm}$. The maximum spatial separation of the nanoparticle (c) is more than 400 nm in the trap. The notation for the horizontal axis of the probability distribution x/x_0 (p/p_0) is adopted from FIG. 4(d) and is used when the oscillator reaches the turning points in the real (momentum) space.

resources from the Holland Computing Center of the University of Nebraska. Funding for this work comes from NSF EPS-1430519 and NSF PHY-1602755.

- [1] L. S. Brown and G. Gabrielse, Rev. Mod. Phys. **58**, 233 (1986).
- [2] D. Hanneke, S. Fogwell, and G. Gabrielse, Phys. Rev. Lett. **100**, 120801 (2008).
- [3] D. Leibfried, R. Blatt, C. Monroe, D. Wineland, Rev. Mod. Phys. **75**, 281 (2003).
- [4] E. A. Cornell and C. E. Wieman, Rev. Mod. Phys. **74**, 875 (2001).
- [5] U. Delić, M. Reisenbauer, K. Dare, D. Grass, V. Vuletić, N. Kiesel, M. Aspelmeyer, Science **367**, 892 (2020).
- [6] E. Schrödinger, Naturwissenschaften **23**, 807 (1935).
- [7] M. Arndt and K. Hornberger, Nat. Phys. **10**, 271 (2014).
- [8] M. Zawisky, M. Baron, R. Loidl, and H. Rauch, Nucl. Instrum. Methods Phys. Res. A **481**, 406 (2002).
- [9] T. Kovachy, P. Asenbaum, C. Overstreet, C. A. Donnelly, S. M. Dickerson, A. Sugarbaker, J. M. Hogan, and M. A. Kasevich, Nature **528**, 530 (2015).
- [10] M. Gebbe, S. Abend, J. -N. Siemß, M. Gersemann, H. Ahlers, H. Müntinga, S. Herrmann, N. Gaaloul, C. Schubert, K. Hammerer, C. Lämmerzahl, W. Ertmer, and E.

- M. Rasel, arXiv:1907.08416 (2019).
- [11] Y. Y. Fein, P. Geyer, P. Zwick, F. Kialka, S. Pedalino, M. Mayor, S. Gerlich, and M. Arndt, *Nat. Phys.* **15**, 1242 (2019).
 - [12] J. Bateman, S. Nimmrichter, K. Hornberger, and H. Ulbricht, *Nat. Commun.* **5**, 4788 (2014).
 - [13] A. Bassi, K. Lochan, S. Satin, T. P. Singh, and H. Ulbricht, *Rev. Mod. Phys.* **85**, 471 (2013).
 - [14] E. Joos, and H. D. Zeh, *Z. Phys. B* **59**, 223 (1985).
 - [15] W. K. Wootters and W. H. Zurek, *Phys. Rev. D* **19**, 473 (1979).
 - [16] W. H. Zurek, *Physics Today* **44**, 36 (1991).
 - [17] S. Bose, A. Mazumdar, G. W. Morley, H. Ulbricht, M. Toroš, M. Paternostro, A. A. Geraci, P. F. Barker, M. S. Kim, and G. Milburn, *Phys. Rev. Lett.* **119**, 240401 (2017).
 - [18] C. Marletto and V. Vedral, *Phys. Rev. Lett.* **119**, 240402 (2017).
 - [19] P. L. Kapitza and P. A. M. Dirac, *Math. Proc. Cambridge Philos. Soc.* **29**, 297 (1933).
 - [20] D. L. Freimund, K. Aflatoon, and H. Batelaan, *Nature* **413**, 142 (2001).
 - [21] D. L. Freimund and H. Batelaan, *Phys. Rev. Lett.* **89**, 283602 (2002).
 - [22] P. L. Gould, G. A. Ruff, and D. E. Pritchard, *Phys. Rev. Lett.* **56**, 827 (1986).
 - [23] P. J. Martin, B. G. Oldaker, A. H. Miklich, and D. E. Pritchard, *Phys. Rev. Lett.* **60**, 515 (1988).
 - [24] T. Pfau, S. Spälter, Ch. Kurtsiefer, C. R. Ekstrom, and J. Mlynek, *Phys. Rev. Lett.* **73**, 1223 (1994).
 - [25] O. Nairz, B. Brezger, M. Arndt, and A. Zeilinger, *Phys. Rev. Lett.* **87**, 160401 (2001).
 - [26] C. Brand, F. Kialka, S. Troyer, C. Knobloch, K. Simonović, B. A. Stickler, K. Hornberger, and M. Arndt, *Phys. Rev. Lett.* **125**, 033604 (2020).
 - [27] W. C. Huang and H. Batelaan, *Atoms* **7**, 42 (2019).
 - [28] Please see derivations and discussions in the supplementary material.
 - [29] H. Batelaan, *Rev. Mod. Phys.* **79**, 929 (2007).
 - [30] O. Smirnova, D. L. Freimund, H. Batelaan, and M. Ivanov, *Phys. Rev. Lett.* **92**, 223601 (2004).
 - [31] S. McGregor, W. C. Huang, B. A. Shadwick, and H. Batelaan, *Phys. Rev. A* **92**, 023834 (2015).
 - [32] M. M. Dellweg and C. Müller, *Phys. Rev. Lett.* **118**, 070403 (2017).
 - [33] W. C. Huang and H. Batelaan, *Found. Phys.* **45**, 333 (2015).
 - [34] M. Kasevich and S. Chu, *Phys. Rev. Lett.* **67**, 181 (1991).
 - [35] M. Kozuma, L. Deng, E. W. Hagley, J. Wen, R. Lutwak, K. Helmerson, S. L. Rolston, and W. D. Phillips, *Phys. Rev. Lett.* **82**, 871 (1999).
 - [36] A. Hemmerich, C. Zimmermann, and T. W. Hänsch, *Phys. Rev. Lett.* **72**, 625 (1994).
 - [37] C. Monroe, D. M. Meekhof, B. E. King, S. R. Jefferts, W. M. Itano, D. J. Wineland, and P. Gould, *Phys. Rev. Lett.* **75**, 4011 (1995).
 - [38] A Sugarbaker, *Atom Interferometry in a 10 m Fountain*. Doctoral thesis, Stanford University (2014).
 - [39] K. E. Cahill and R. J. Glauber, *Phys. Rev.* **177**, 1857 (1969).
 - [40] D. J. Wineland, C. Monroe, W. M. Itano, B. E. King, D. Leibfried, D. M. Meekhof, C. Myatt, and C. Wood, *Fortschr. Phys.* **46**, 363 (1998).
 - [41] A. Caprez, R. Bach, S. McGregor, and H. Batelaan, *J. Phys. B: At. Mol. Opt. Phys.* **42**, 165503 (2009).
 - [42] F. Hasselbach, *Rep. Prog. Phys.* **73**, 016101 (2010).
 - [43] F. S. Yasin, K. Harada, D. Shindo, H. Shinada, B. J. McMorran, and T. Tanigaki, *Appl. Phys. Lett.* **113**, 233102 (2018).
 - [44] S.-w. Chiow, T. Kovachy, H. -C. Chien, and M. A. Kasevich, *Phys. Rev. Lett.* **107**, 130403 (2011).
 - [45] J. Rudolph, T. Wilkason, M. Nantel, H. Swan, C. M. Holland, Y. Jiang, B. E. Garber, S. P. Carman, and Jason M. Hogan, *Phys. Rev. Lett.* **124**, 083604 (2020).
 - [46] D. M. Giltner, R. W. McGowan, and S. A. Lee, *Phys. Rev. Lett.* **75**, 2638 (1995).
 - [47] B. Vlastakis, G. Kirchmair, Z. Leghtas, S. E. Nigg, L. Frunzio, S. M. Girvin, M. Mirrahimi, M. H. Devoret, and R. J. Schoelkopf, *Science* **342**, 607 (2013).
 - [48] M. Hofheinz, H. Wang, M. Ansmann, R. C. Bialczak, E. Lucero, M. Neeley, A. D. O'Connell, D. Sank, J. Wenner, John M. Martinis, and A. N. Cleland, *Nature* **459**, 546 (2009).
 - [49] K.G. Johnson, J.D. Wong-Campos, B. Neyenhuis, J. Mizrahi, and C. Monroe, *Nat. Commun.* **8**, 697 (2017).
 - [50] S. Gerlich, S. Eibenberger, M. Tomandl, S. Nimmrichter, K. Hornberger, P. J. Fagan, J. Tüxen, M. Mayor, and M. Arndt, *Nat. Comm.* **2**, 263 (2011).

Supplementary Material

Wayne Cheng-Wei Huang,¹ Herman Batelaan,² and Markus Arndt³

¹*Department of Physics and Astronomy, Northwestern University, Evanston, Illinois 60208, USA*

²*Department of Physics and Astronomy, University of Nebraska-Lincoln, Lincoln, Nebraska 68588, USA*

³*Faculty of Physics, University of Vienna, Boltzmannngasse 5, A-1090 Vienna, Austria*

This supplementary material is aimed for providing a detailed account of the inelastic Kapitza-Dirac (KD) scattering as presented in the main text. Additionally, we extend the analysis to 2D and 3D harmonic oscillators and show that not only KD blockade persists to work with added dimensionality, but the possibility of entanglement also arises.

I. Derivation of the dimensionless transition amplitude $g_n(\eta)$ in *inelastic* Kapitza-Dirac scattering

(a) *An electron in a 1D pondermotive trap*

We consider a free electron interacting with two pairs of counter-propagating laser fields as shown in FIG. 1. The electron travels in the z -direction, and the laser fields propagate in the x -direction. Both pairs of laser fields are pulsed. The first pair of fields has the same frequency ω_{TL} and form a standing wave with a linear polarization along the y -axis. The second pair of fields are running waves with different frequencies $\omega_{1,2}$ ($\omega_1 > \omega_2$) and a linear polarization along the z -axis. The quantum Hamilton of the electron is

$$\begin{aligned}\hat{H} &= \frac{(\mathbf{p} - q_e \mathbf{A})^2}{2m_e} \\ &= \frac{\mathbf{p}^2}{2m_e} - \frac{q_e}{2m_e} \mathbf{p} \cdot \mathbf{A} - \frac{q_e}{2m_e} \mathbf{A} \cdot \mathbf{p} + \frac{q_e^2}{2m_e} \mathbf{A}^2,\end{aligned}\quad (1)$$

where $\mathbf{p} = -i\hbar\nabla$ and $\mathbf{A} = \mathbf{A}_{\text{TL}} + \mathbf{A}_1 + \mathbf{A}_2$. We use $q_e = -e$ and m_e as electron charge and mass. The vector potential \mathbf{A}_{TL} of the standing wave is

$$\mathbf{A}_{\text{TL}}(x, t) = \sqrt{\frac{2I_s}{\epsilon_0 c \omega_{\text{TL}}^2}} \exp(-t^2/\tau_{\text{TL}}^2) \cos(k_{\text{TL}}x) \cos(\omega_{\text{TL}}t) \vec{e}_y, \quad (2)$$

where $k_{\text{TL}} = \omega_{\text{TL}}/c$ and I_s is the intensity of the standing wave at the center of the waist. Note that the individual trapping laser beam in the standing wave has a pulse intensity $I_{\text{TL}} = I_s/4$ and the $1/e$ pulse duration τ_{TL} . We denote x as the particle position operator hereafter. The pair of counter-propagating running waves are called KD lasers, and their vector potential $\mathbf{A}_{1,2}$ are

$$\mathbf{A}_{1,2}(x, t) = A_{1,2} \exp(-t^2/\tau_{\text{KD}}^2) \cos(-k_{1,2}x \pm \omega_{1,2}t) \vec{e}_z, \quad (3)$$

where $A_{1,2} = \sqrt{2I_{\text{KD}}/\epsilon_0 c \omega_{1,2}^2}$, $k_{1,2} = \omega_{1,2}/c$, I_{KD} is the intensity of individual KD lasers at the center of the waist, and τ_{KD} is the $1/e$ pulse duration. Here we approximate all laser fields to be homogenous over the area of interaction

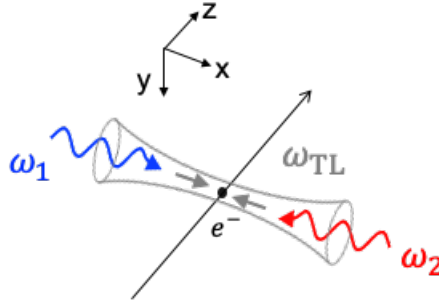


FIG. 1. (color online) An electron interacting with a standing wave (gray) of frequency ω_{TL} and two counter-propagating laser fields of frequencies $\omega_{1,2}$ (blue and red).

in the y - z plane. This approximation is justified when (1) the laser beam sizes in the y -direction are much larger than the electron beam size along the same direction, and (2) the laser beam sizes in the z -direction satisfy the relation

$$\tau_{\text{TL}} \gg \frac{W_{z\text{-TL}}}{2v_z} \gg \frac{W_{z\text{-KD}}}{2v_z} \gg \tau_{\text{KD}}, \quad (4)$$

where w_z is the $1/e$ beam diameter along the z -axis, and v_z is the electron's speed along the z -axis. The subscripts -TL and -KD denote the trapping and the KD lasers respectively.

The first term in Eq. (1) is the electron kinetic energy. The second term in Eq. (1) is simplified to be $\mathbf{p} \cdot \mathbf{A} = (-i\hbar\nabla) \cdot \mathbf{A} + \mathbf{A} \cdot (-i\hbar\nabla) = \mathbf{A} \cdot \mathbf{p}$ in the Coulomb gauge $\nabla \cdot \mathbf{A} = 0$. Thus it can be combined with the third term $\mathbf{A} \cdot \mathbf{p}$. At the first-order, the $\mathbf{A} \cdot \mathbf{p}$ term corresponds to single-photon scatterings which do not conserve energy and momentum for electrons. However, at the second order the $\mathbf{A} \cdot \mathbf{p}$ term can give rise to wave mixing and result in resonant scattering. From a classical analysis [1], it can be shown that the combined action of the $\mathbf{A} \cdot \mathbf{p}$ term and the \mathbf{A}^2 term in Eq. (1) is equivalent to keeping only the \mathbf{A}^2 term in Eq. (1). Since the polarizations of the standing wave and the running waves are orthogonal $\mathbf{A}_{\text{TL}} \cdot \mathbf{A}_{1,2} = 0$, the \mathbf{A}^2 term can be expanded as $\mathbf{A}^2 = \mathbf{A}_{\text{TL}}^2 + \mathbf{A}_1^2 + \mathbf{A}_2^2 + 2\mathbf{A}_1 \cdot \mathbf{A}_2$ and the Hamiltonian in Eq. (1) can be rewritten as

$$\hat{H} = \frac{\mathbf{p}^2}{2m_e} + \frac{q_e^2}{2m_e} (\mathbf{A}_{\text{TL}}^2 + \mathbf{A}_1^2 + \mathbf{A}_2^2 + 2\mathbf{A}_1 \cdot \mathbf{A}_2). \quad (5)$$

Assuming that the standing wave is much stronger than the running waves, $|\mathbf{A}_{\text{TL}}| \gg |\mathbf{A}_{1,2}|$, the Hamiltonian can be separated into an unperturbed part

$$\hat{H}_0 = \frac{\mathbf{p}^2}{2m_e} + \frac{q_e^2 \mathbf{A}_{\text{TL}}^2}{2m_e}, \quad (6)$$

and an interaction part

$$\hat{H}_{\text{int}} = \frac{q_e^2}{2m_e} (\mathbf{A}_1^2 + \mathbf{A}_2^2 + 2\mathbf{A}_1 \cdot \mathbf{A}_2). \quad (7)$$

Using Eq. (2), the unperturbed Hamiltonian can be written as $\hat{H}_0 = \mathbf{p}^2/2m_e + U(x, t)$, where

$$U(x, t) = \frac{q_e^2 I_s}{2\epsilon_0 c \omega_{\text{TL}}^2 m_e} \exp(-2t^2/\tau_{\text{TL}}^2) \cos^2(k_{\text{TL}} x) (1 + \cos(2\omega_{\text{TL}} t)). \quad (8)$$

The first term in Eq. (8) is time-dependent, while the second term with $\cos(2\omega_{\text{TL}} t)$ can be discarded because it only causes non-resonant driving and the effect averages out. Thus, we obtain the pondermotive potential for the well-known elastic KD scattering,

$$U_p(x) = \frac{q_e^2 I_s}{2\epsilon_0 c \omega_{\text{TL}}^2 m_e} \cos^2(k_{\text{TL}} x), \quad (9)$$

where the Gaussian-shaped time envelope is approximated as $\exp(-2t^2/\tau_{\text{TL}}^2) \approx 1$ because it is slow-varying during the interaction time τ_{KD} . Depending on the relation between the potential strength $U_0 = q_e^2 I_s / 2\epsilon_0 c \omega_{\text{TL}}^2 m_e$, the recoil energy $E_R = \hbar^2 (2k_{\text{TL}})^2 / 2m_e$, and the transit time $\Delta t = W_{z\text{-TL}} / v_z$, there are three parameter regimes of interaction: (1) diffraction regime ($E_R \ll \hbar/\Delta t$, $E_R \ll U_0$), (2) Bragg regime ($E_R \gg \hbar/\Delta t$, $E_R \gg U_0$), and (3) channeling regime ($U_0 \gg E_R \gg \hbar/\Delta t$) [5]. We assume that the experimental parameters are chosen for interaction in the channeling regime, so that the electron is transversely confined by the pondermotive potential as it travels through the standing wave. Close to the potential minimum $x_m = \lambda_{\text{TL}}/4$, where $\lambda_{\text{TL}} = 2\pi/k_{\text{TL}}$, the pondermotive potential can be approximated as a harmonic trap

$$U_p(x) \approx \frac{1}{2} \left(\frac{q_e^2 I_s}{\epsilon_0 c^3 m_e} \right) x^2 = \frac{1}{2} m_e \Omega_0^2 x^2, \quad (10)$$

where x is repurposed to denote the displacement from the potential minimum x_m , and the trap frequency is

$$\Omega_0 = \sqrt{\frac{q_e^2 I_s}{\epsilon_0 c^3 m_e^2}}. \quad (11)$$

Therefore, the unperturbed Hamiltonian in Eq. (6) becomes

$$\hat{H}_0 = \left(\frac{p_x^2}{2m_e} + \frac{1}{2}m_e\Omega_0^2 x^2 \right) + \frac{p_y^2 + p_z^2}{2m_e}, \quad (12)$$

where $(p_x, p_y, p_z) \equiv -i\hbar(\partial/\partial x, \partial/\partial y, \partial/\partial z)$. Thus, for parameters in the channeling regime the x -motion of the electron is confined in an 1D harmonic trap while the y - and z -motions freely propagate. The general solution to the electron's wavefunction is

$$|\psi\rangle(t) = \phi(y, z, t) \left(\sum_{n=0}^{\infty} C_n(t) e^{-i\Omega_n t} |n\rangle \right), \quad (13)$$

where $\phi(y, z, t)$ is the wavefunction of a free wavepacket, and $\Omega_n \equiv \Omega_0(n + 1/2)$ characterizes the excitation of the harmonic oscillator in the x -direction. We are interested in solving the probability amplitude $C_n(t)$ for each eigenstate $|n\rangle$ of the harmonic oscillator. Using Eq. (3), the interaction Hamiltonian in Eq. (7) can be expanded as

$$\begin{aligned} \hat{H}_{int} = & \frac{q_e^2}{2m_e} \exp(-2t^2/\tau_{KD}^2) [A_1^2 \cos^2(k_1 x - \omega_1 t) + A_2^2 \cos^2(k_2 x + \omega_2 t)] \\ & + \frac{q_e^2}{2m_e} A_1 A_2 \exp(-2t^2/\tau_{KD}^2) [\cos((k_1 + k_2)x - (\omega_1 - \omega_2)t) + \cos((k_1 - k_2)x - (\omega_1 + \omega_2)t)], \end{aligned} \quad (14)$$

and the corresponding Schrödinger equation for $C_n(t)$ is

$$i\hbar \frac{dC_m(t)}{dt} = \sum_{n=0}^{\infty} \langle m | \hat{H}_{int} | n \rangle C_n(t) e^{i\Omega_{mn} t}, \quad (15)$$

where $\Omega_{mn} \equiv \Omega_m - \Omega_n$. To analyze the excitation dynamics, we group Eq. (15) into even and odd transitions,

$$\begin{aligned} i\hbar \frac{dC_m(t)}{dt} = & \sum_{n=0}^{\infty} \left(\langle m | \hat{H}_{int} | m - 2n \rangle C_{m-2n}(t) e^{i2n\Omega_0 t} + \langle m | \hat{H}_{int} | m + 2n \rangle C_{m+2n}(t) e^{-i2n\Omega_0 t} \right) \\ & + \sum_{n=0}^{\infty} \left(\langle m | \hat{H}_{int} | m - (2n + 1) \rangle C_{m-(2n+1)}(t) e^{i(2n+1)\Omega_0 t} + \langle m | \hat{H}_{int} | m + (2n + 1) \rangle C_{m+(2n+1)}(t) e^{-i(2n+1)\Omega_0 t} \right). \end{aligned} \quad (16)$$

The terms in the first summation represent even transitions, while those in the second summation represent odd transitions. Assuming that $\omega_{1,2}$ are many orders of magnitude higher than Ω_0 , only the $\omega_1 - \omega_2$ term in Eq. (14) can resonantly excite the oscillator, which leads to a simplification of Eq. (14),

$$\begin{aligned} \hat{H}_{int} = & \frac{q_e^2}{4m_e} A_1 A_2 \exp(-2t^2/\tau_{KD}^2) \cos((k_1 + k_2)x) \left(e^{i(\omega_1 - \omega_2)t} + e^{-i(\omega_1 - \omega_2)t} \right) \\ & - i \frac{q_e^2}{4m_e} A_1 A_2 \exp(-2t^2/\tau_{KD}^2) \sin((k_1 + k_2)x) \left(e^{i(\omega_1 - \omega_2)t} - e^{-i(\omega_1 - \omega_2)t} \right), \end{aligned} \quad (17)$$

where $\cos((\omega_1 - \omega_2)t)$ and $\sin((\omega_1 - \omega_2)t)$ are expanded. In Eq. (17), the first term with $\cos((k_1 + k_2)x)$ gives rise to even transitions $|n\rangle \rightarrow |n \pm 2k\rangle$, where k is a positive integer. This is because the position operator of a harmonic oscillator can be expressed in terms of the rising and lowering operators, $x = x_0(\hat{b}^\dagger + \hat{b})$, where $x_0 = \sqrt{\hbar/2m_e\Omega_0}$, $\hat{b}^\dagger|n\rangle = \sqrt{n+1}|n+1\rangle$, and $\hat{b}|n\rangle = \sqrt{n}|n-1\rangle$. The expansion of $\cos((k_1 + k_2)x)$ contains only even powers of \hat{b}^\dagger and \hat{b} . The resonant excitation frequency for even transitions $|n\rangle \rightarrow |n \pm 2k\rangle$ is $\omega_1 - \omega_2 = 2k\Omega_0$ because $e^{\pm i(\omega_1 - \omega_2)t} = e^{\pm i2k\Omega_0 t}$ in Eq. (17) cancel with $e^{\mp i2n\Omega_0 t}$ in Eq. (16) for $n = k$. Similarly, the $\sin((k_1 + k_2)x)$ term gives rise to the odd transitions, and the corresponding excitation frequency is $\omega_1 - \omega_2 = (2k + 1)\Omega_0$.

The above observation can also be derived from the basis of parametric resonance. Let us switch to the interaction picture and replace the position operator x in Eq. (17) by $x(t)$,

$$x \longrightarrow x(t) = \sqrt{\frac{\hbar}{2m_e\Omega_0}} \left(\hat{b}^\dagger e^{i\Omega_0 t} + \hat{b} e^{-i\Omega_0 t} \right). \quad (18)$$

To obtain the frequency components of $\cos((k_1 + k_2)x)$ and $\sin((k_1 + k_2)x)$ in Eq. (17), we first find the frequency components in $x^m(t)$ using the binomial expansion,

$$x^m(t) = \left(\sqrt{\frac{\hbar}{2m_e\Omega_0}} \right)^m \sum_{n=0}^m e^{-i(m-2n)\Omega_0 t} \binom{m}{n} \hat{b}^\dagger{}^n \hat{b}^{(m-n)}. \quad (19)$$

The frequency components, $|m - 2n|\Omega_0$, are either even or odd depending on the power m . Since there are only even powers of $x(t)$ in $\cos((k_1 + k_2)x)$, the frequency components in $\cos((k_1 + k_2)x)$ are all even. Similarly, the frequency components in $\sin((k_1 + k_2)x)$ are all odd. Given the excitation frequency $\omega_1 - \omega_2 = 2k\Omega_0$, there will be some frequency components in $\cos((k_1 + k_2)x)$ that cancel with $e^{\pm i(\omega_1 - \omega_2)t}$ and lead to parametric excitation. On the other hand, because $\cos((k_1 + k_2)x)$ contains only even powers of \hat{b}^\dagger and \hat{b} , the transitions involved in parametric excitation at $\omega_1 - \omega_2 = 2k\Omega_0$ are all even.

A rigorous and general proof can be obtained by examining the transition matrix element of the interaction Hamiltonian in Eq. (17),

$$\langle m | \hat{H}_{int} | n \rangle = f(t) \langle m | \cos((k_1 + k_2)x) | n \rangle + h(t) \langle m | \sin((k_1 + k_2)x) | n \rangle, \quad (20)$$

where

$$\begin{aligned} f(t) &\equiv (q_e^2/2m_e) A_1 A_2 \exp(-2t^2/\tau_{\text{KD}}^2) \cos((\omega_1 - \omega_2)t), \\ h(t) &\equiv (q_e^2/2m_e) A_1 A_2 \exp(-2t^2/\tau_{\text{KD}}^2) \sin((\omega_1 - \omega_2)t). \end{aligned} \quad (21)$$

We can find $\langle m | \cos((k_1 + k_2)x) | n \rangle$ and $\langle m | \sin((k_1 + k_2)x) | n \rangle$ by first evaluating the matrix element

$$\langle m | e^{i(k_1 + k_2)x} | n \rangle = \int_{-\infty}^{\infty} dx \phi_m^*(x) e^{i(k_1 + k_2)x} \phi_n(x), \quad (22)$$

where $\phi_m(x)$ is an eigen-wavefunction of the harmonic oscillator in real space. Using the convolution theorem

$$\int_{-\infty}^{\infty} dx \phi_1^*(x) \phi_2(x) e^{ik'x} = 2\pi \int_{-\infty}^{\infty} dk \psi_1^*(k) \psi_2(k - k'), \quad (23)$$

where $\psi_{1,2}(k) = (1/2\pi) \int_{-\infty}^{\infty} dx \phi_{1,2}(x) e^{-ikx}$, Eq. (22) can be transformed to

$$\langle m | e^{i(k_1 + k_2)x} | n \rangle = \int_{-\infty}^{\infty} dk \psi_m^*(k) \psi_n(k - (k_1 + k_2)). \quad (24)$$

Here we remark that Eq. (24) depicts the essential element in both elastic and inelastic KD scattering — a periodic potential gives rise to momentum kicks. While Eq. (24) is general and valid for both free particles and harmonic oscillators, in the case of harmonic oscillators, there is one additional property due to the parity of the oscillator eigenstates $|m\rangle$ and $|n\rangle$,

$$\int_{-\infty}^{\infty} dk \psi_m^*(k) \psi_n(k - (k_1 + k_2)) = (-1)^{(m+n)} \int_{-\infty}^{\infty} dk \psi_m^*(k) \psi_n(k + (k_1 + k_2)). \quad (25)$$

The physical interpretation of Eq. (25) is that for harmonic oscillators the transition amplitudes for stimulated emission (the integral with $\psi_n(k + (k_1 + k_2))$) and absorption (the integral with $\psi_n(k - (k_1 + k_2))$) are equal in strength but differ by a phase factor of the parity change $(-1)^{m+n}$. Using Eqs. (24) and (25), the transition matrix element in Eq. (20) can be evaluated as

$$\langle m | \hat{H}_{int} | n \rangle = \pi [f(t) (1 + (-1)^{m+n}) - ih(t) (1 - (-1)^{m+n})] \int_{-\infty}^{\infty} dk \psi_m^*(k) \psi_n(k - (k_1 + k_2)). \quad (26)$$

For even transitions $m = n + 2k$, where k is a positive integer, Eq. (26) becomes

$$\langle n + 2k | \hat{H}_{int} | n \rangle = 2\pi f(t) \int_{-\infty}^{\infty} dk \psi_{n+2k}^*(k) \psi_n(k - (k_1 + k_2)) = f(t) \langle n + 2k | \cos((k_1 + k_2)x) | n \rangle. \quad (27)$$

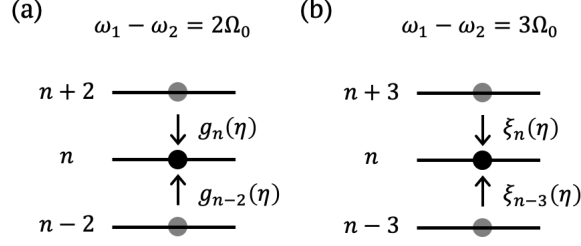


FIG. 2. A schematic for the transition processes with (a) $\omega_1 - \omega_2 = 2\Omega_0$ and (b) $\omega_1 - \omega_2 = 3\Omega_0$.

For odd transition $m = n + 2k + 1$, Eq. (26) becomes

$$\langle n + 2k + 1 | \hat{H}_{int} | n \rangle = -i2\pi\hbar(t) \int_{-\infty}^{\infty} dk \psi_{n+2k+1}^*(k) \psi_n(k - (k_1 + k_2)) = \hbar(t) \langle n + 2k + 1 | \sin((k_1 + k_2)x) | n \rangle. \quad (28)$$

If $\omega_1 - \omega_2 = 2k\Omega_0$, it can be shown from Eq. (16) that only even transitions are resonantly driven. Their transition matrix elements can be evaluated by Eq. (27) which involves only the $\cos((k_1 + k_2)x)$ term in Eq. (17). Similarly, in the case of $\omega_1 - \omega_2 = (2k + 1)\Omega_0$ only the $\sin((k_1 + k_2)x)$ term in Eq. (17) is involved in the resonant excitation. With Eqs. (16) and (26), we can summarize the conditions for resonant excitation in terms of energy-momentum conservation,

$$\begin{cases} \omega_1 - \omega_2 = n_e \Omega_0 \\ k_1 + k_2 = (n_e + \delta_p) k_0, \end{cases} \quad (29)$$

where $k_0 = \sqrt{m_e \Omega_0 / 2\hbar}$, n_e is a positive integer, and $\delta_p \geq -n_e$ is the momentum detuning discussed in the main text.

The energy-momentum relation in Eq. (29) and the transition amplitudes in Eqs. (27) and (28) together give a clear physical picture of the inelastic KD scattering as an oscillator receiving a momentum kick $\hbar(k_1 + k_2)$ and making a transition to a higher energy level. This picture allows us to give a physical interpretation for the KD blockade mechanism as described in FIG. 2 of the main text. However, the integral form of Eqs. (27) and (28) are impractical to implement in numerical simulations, especially when the number of the involved eigenstates is large. Additionally, to identify the exact value of the momentum detuning δ_p for KD blockade, it is desirable to derive the analytic forms for Eqs. (27) and (28). Cahill and Glauber [2] have shown that for a harmonic oscillator,

$$\langle m | e^{i(k_1 + k_2)x} | n \rangle = \sqrt{\frac{n!}{m!}} (i\eta)^{m-n} e^{-\eta^2/2} L_n^{(m-n)}(\eta^2) \quad \text{for } m > n, \quad (30)$$

where $\eta \equiv (k_1 + k_2)x_0$ is the Lamb-Dicke parameter, and $L_n^{(m-n)}(y)$ is the generalized Laguerre polynomial. This equation gives Eqs. (27) and (28) the desired analytic forms,

$$\begin{aligned} \langle n + 2k | \cos((k_1 + k_2)x) | n \rangle &= \sqrt{\frac{n!}{(n + 2k)!}} (-1)^k \eta^{2k} e^{-\eta^2/2} L_n^{(2k)}(\eta^2), \\ \langle n + 2k + 1 | \sin((k_1 + k_2)x) | n \rangle &= \sqrt{\frac{n!}{(n + 2k + 1)!}} (-1)^k \eta^{2k+1} e^{-\eta^2/2} L_n^{(2k+1)}(\eta^2). \end{aligned} \quad (31)$$

So far we have been discussing the general theory of the inelastic KD scattering. Let us apply these results to the specific cases discussed in the main text. In the case of $\omega_1 - \omega_2 = 2\Omega_0$, which is used in the main text to populate a single eigenstate $|n = 2\rangle$ and to prepare a Schrödinger cat state, the interaction Hamiltonian in Eq. (17) is reduced to

$$\hat{H}_{int} = f(t) \cos((k_1 + k_2)x), \quad (32)$$

where $f(t)$ is given in Eq. (21). Note that this interaction Hamiltonian is the effective KD potential $V_{KD}(\hat{x}, t)$ in the main text. Using Eq. (31), we define the dimensionless transition amplitude

$$g_n(\eta) \equiv \langle n + 2 | \cos((k_1 + k_2)x) | n \rangle = -\sqrt{\frac{n!}{(n + 2)!}} \eta^2 L_n^{(2)}(\eta^2) e^{-\eta^2/2}. \quad (33)$$

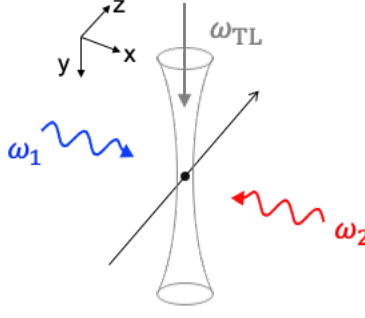


FIG. 3. (color online) A polarizable neutral particle trapped in the x -direction by the gradient force of a focused laser beam (gray) interacts with two counter-propagating laser fields of frequencies $\omega_{1,2}$ (blue and red).

Therefore, according to Eq. (16) the corresponding Schrödinger equation is

$$i\hbar \frac{dC_n(t)}{dt} = f(t) (g_{n-2}(\eta)C_{n-2}(t)e^{i2\Omega_0 t} + g_n(\eta)C_{n+2}(t)e^{-i2\Omega_0 t}), \quad (34)$$

where hermiticity is used to give $\langle n+2|\hat{H}_{int}|n\rangle = \langle n|\hat{H}_{int}|n+2\rangle$. We note that even in the Lamb-Dicke regime $\eta \ll 1$, the inelastic KD scattering as described in Eq. (34) can still be driven. For $\omega_1 - \omega_2 = 3\Omega_0$, which is used in the main text to prepare a 3-component Schrödinger cat state, the interaction Hamiltonian in Eq. (17) is reduced to

$$\hat{H}_{int} = h(t) \sin((k_1 + k_2)x). \quad (35)$$

The dimensionless transition amplitude $\xi_n(\eta) \equiv \langle n+3|\sin((k_1 + k_2)x)|n\rangle = -\sqrt{n!/(n+3)!}\eta^3 L_n^{(3)}(\eta^2)e^{-\eta^2/2}$ is used to identify the proper momentum detuning $\delta_p = -1.57$ for the KD blockade at $|n| = 18$. The corresponding Schrödinger equation is

$$i\hbar \frac{dC_n(t)}{dt} = h(t) (\xi_{n-3}(\eta)C_{n-3}(t)e^{i3\Omega_0 t} + \xi_n(\eta)C_{n+3}(t)e^{-i3\Omega_0 t}). \quad (36)$$

In FIG. 2, we give an illustration for the transition processes in Eqs. (34) and (36).

(b) A polarizable particle in a 1D dipole trap

Next, we consider the interaction between a pair of counter-propagating laser fields and a polarizable neutral particle (i.e. atoms, molecules, and dielectric nanoparticles) in a 1D optical trap. A schematic is shown in FIG. 3. In contrast to the electron setup, here the lasers are continuous-wave instead of pulsed. This is because the time scale of dynamics as determined by the trap frequency is much longer for massive particles compared to electrons. Polarizable neutral particles interact with laser fields through the dipole force, so the quantum Hamiltonian is

$$\hat{H} = \frac{\mathbf{p}^2}{2M} - \frac{1}{2}\alpha\mathbf{E}^2, \quad (37)$$

where α and M are the polarizability and mass of the particle, and $\mathbf{E} = \mathbf{E}_{TL} + \mathbf{E}_1 + \mathbf{E}_2$. For most large molecules and dielectric nanoparticles, the optical polarizability is approximately equal to the static polarizability. For atoms, the near-resonant enhancement in the optical polarizability can be used as a tuning parameter. Expanding Eq. (37) gives

$$\hat{H} = \frac{\mathbf{p}^2}{2M} - \frac{1}{2}\alpha(\mathbf{E}_{TL}^2 + \mathbf{E}_1^2 + \mathbf{E}_2^2 + 2\mathbf{E}_1 \cdot \mathbf{E}_2). \quad (38)$$

Trapping for polarizable neutral particles in the x -direction requires only one laser beam instead of a standing wave. The electric field of the trapping laser is

$$\begin{aligned} \mathbf{E}_{TL}(x, y, z, t) &= \sqrt{\frac{2I_{TL}}{\epsilon_0 c}} \exp\left(-\frac{4x^2}{W_{x-TL}^2} - \frac{4z^2}{W_{z-TL}^2}\right) \cos(k_{TL}y - \omega_{TL}t) \vec{e}_x \\ &= \sqrt{\frac{2I_{TL}}{\epsilon_0 c}} \exp\left(-\frac{4x^2}{W_{x-TL}^2}\right) \exp\left[\frac{-t^2}{(W_{z-TL}/2v_z)^2}\right] \cos(k_{TL}y - \omega_{TL}t) \vec{e}_x, \end{aligned} \quad (39)$$

where $W_{x\text{-TL}}$ and $W_{z\text{-TL}}$ are the $1/e$ beam diameters in the x - and z -directions, and v_z is the particle's speed along the z -axis. The electric fields of the KD lasers are

$$\mathbf{E}_{1,2}(x, t) = E_{1,2} \exp(-t^2/\tau_{\text{KD}}^2) \cos(-k_{1,2}x \pm \omega_{1,2}t) \vec{e}_z, \quad (40)$$

where $E_{1,2} = \sqrt{2I_{\text{KD}}/\epsilon_0 c}$. The KD laser pulse duration τ_{KD} controls the interaction time, and it can be set by an acoustic optical modulator. As in Eqs. (2) and (3), we approximate both the trapping and the KD lasers to be homogeneous in the y -direction, assuming that the length scale of intensity variation is much larger than the particle beam size along the same direction. We also approximate the KD laser fields to be homogeneous in the z -direction according to the criteria given in Eq. (4). Because the transit time $W_{z\text{-TL}}/v_z$ is assumed to be much longer than the interaction time $2\tau_{\text{KD}}$, we can approximate $\exp[-t^2/(W_{z\text{-TL}}/2v_z)^2] \approx 1$ and rewrite Eq. (39) as

$$\mathbf{E}_{\text{TL}}(x, y, z, t) = \sqrt{\frac{2I_{\text{TL}}}{\epsilon_0 c}} \exp\left(-\frac{4x^2}{W_{x\text{-TL}}^2}\right) \cos(k_{\text{TL}}y - \omega_{\text{TL}}t) \vec{e}_x. \quad (41)$$

Assuming that the trapping laser is much stronger than the KD lasers, $|\mathbf{E}_{\text{TL}}| \gg |\mathbf{E}_{1,2}|$, the Hamiltonian can be separated into an unperturbed part

$$\hat{H}_0 = \frac{\mathbf{p}^2}{2M} - \frac{1}{2}\alpha \mathbf{E}_{\text{TL}}^2, \quad (42)$$

and an interaction part

$$\hat{H}_{\text{int}} = -\frac{1}{2}\alpha(\mathbf{E}_1^2 + \mathbf{E}_2^2 + 2\mathbf{E}_1 \cdot \mathbf{E}_2). \quad (43)$$

Using Eq. (41), we can write down a trapping potential for the unperturbed Hamiltonian in Eq. (42),

$$U(x, t) = -\frac{1}{2}\alpha \mathbf{E}_{\text{TL}}^2 = -\frac{1}{2} \frac{\alpha I_{\text{TL}}}{\epsilon_0 c} \exp(-8x^2/W_{x\text{-TL}}^2) (1 + \cos(2k_{\text{TL}}y - 2\omega_{\text{TL}}t)). \quad (44)$$

The first term in Eq. (44) is time-independent. Assuming ω_{TL} to be far from any electronic resonance of the particle, the second term $\cos(2k_{\text{TL}}y - 2\omega_{\text{TL}}t)$ in Eq. (44) can be discarded because it only causes non-resonant driving and the effect averages out. As a result, we obtain the dipole potential from Eq. (44),

$$U_d(x) = -\frac{1}{2} \frac{\alpha I_{\text{TL}}}{\epsilon_0 c} \exp(-8x^2/W_{x\text{-TL}}^2). \quad (45)$$

Close to the potential minimum $x_m = 0$, the potential in Eq. (45) can be approximated as a harmonic trap

$$U_d(x) \approx \frac{1}{2} \frac{8\alpha I_{\text{TL}}}{\epsilon_0 c W_{x\text{-TL}}^2} x^2, \quad (46)$$

where a constant in the expansion is dropped out, and the trap frequency is

$$\Omega_0 = \sqrt{\frac{8\alpha I_{\text{TL}}}{\epsilon_0 c M W_{x\text{-TL}}^2}}. \quad (47)$$

Thus, the unperturbed Hamiltonian in Eq. (42) becomes

$$\hat{H}_0 = \left(\frac{p_x^2}{2M} + \frac{1}{2} M \Omega_0^2 x^2 \right) + \frac{p_y^2 + p_z^2}{2M}. \quad (48)$$

Since Eq. (48) is the same as Eq. (12), the general solution to the particles' wavefunction is also described by Eq. (13). We can examine the interaction between the KD lasers and the oscillator by evaluating Eq. (43),

$$\begin{aligned} \hat{H}_{\text{int}} = & -\frac{\alpha}{2} \exp(-2t^2/\tau_{\text{KD}}^2) [E_1^2 \cos^2(k_1x - \omega_1t) + E_2^2 \cos^2(k_2x + \omega_2t)] \\ & - \frac{\alpha}{2} E_1 E_2 \exp(-2t^2/\tau_{\text{KD}}^2) [\cos((k_1 + k_2)x - (\omega_1 - \omega_2)t) + \cos((k_1 - k_2)x - (\omega_1 + \omega_2)t)], \end{aligned} \quad (49)$$

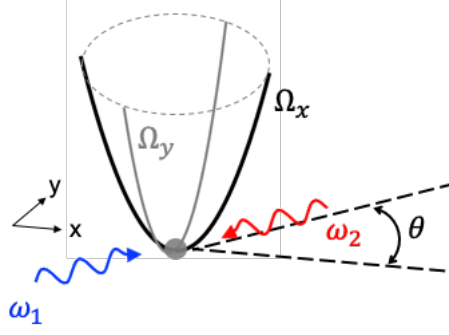


FIG. 4. (color online) A 3D harmonic oscillator interacting with the KD laser fields in the xy -plane.

which has the same form as Eq. (14). Comparing Eqs. (48) and (49) to Eqs. (12) and (14), we see that the only difference is a direct replacement of coefficients,

$$\begin{aligned} m_e &\longrightarrow M \\ A_{1,2} &\longrightarrow E_{1,2} \\ \frac{q_e^2}{2m_e} &\longrightarrow -\frac{\alpha}{2}. \end{aligned} \quad (50)$$

Therefore, all the analysis and results from Eq. (15) to Eq. (36) apply for polarizable neutral particles.

(c) *Extension to 2D and 3D harmonic traps*

We now extend our discussion to particles in 2D and 3D harmonic traps, which are common for atoms, ions, molecules, and dielectric nanoparticles. The analysis presented here focuses on 3D harmonic oscillators but the results can be adapted for 2D harmonic oscillators. Let us consider a non-degenerate 3D harmonic oscillator with trap frequencies $(\Omega_x, \Omega_y, \Omega_z)$ along the x -, y -, and z -axes. We extend the unperturbed Hamiltonian in Eq. (48) to 3D,

$$\hat{H}_0 = \left(\frac{p_x^2}{2M} + \frac{1}{2}M\Omega_x^2 x^2 \right) + \left(\frac{p_y^2}{2M} + \frac{1}{2}M\Omega_y^2 y^2 \right) + \left(\frac{p_z^2}{2M} + \frac{1}{2}M\Omega_z^2 z^2 \right). \quad (51)$$

The oscillator is assumed to be initially in the ground state $|0\rangle_x |0\rangle_y |0\rangle_z$, where $|n\rangle_{x,y,z}$ are the eigenstates of the 3D harmonic oscillator along the x -, y -, and z -axes. We define these three degrees of freedoms as the x -, y -, and z -oscillators hereafter. If the KD lasers propagate along the x -axis, only the x -oscillator can be resonantly excited. The general solution to the oscillator's wavefunction is

$$|\psi\rangle(t) = |0\rangle_y e^{-i\Omega_y t/2} |0\rangle_z e^{-i\Omega_z t/2} \left(\sum_{n=0}^{\infty} C_n(t) e^{-i\Omega_n t} |n\rangle_x \right), \quad (52)$$

where $\Omega_n \equiv \Omega_x(n + 1/2)$. Since the dynamics of $C_n(t)$ pertains to only the x -oscillator, the analysis from the previous subsection applies here.

When the KD lasers travel in an oblique angle with respect to the potential axes, different degrees of freedom of the 3D harmonic oscillator can interact with the KD laser fields at the same time and this leads to entanglement. As an example, we consider KD laser fields traveling in the xy -plane with wavevectors $\mathbf{k}_{1,2} = \pm (\cos(\theta), \sin(\theta), 0) \omega_{1,2}/c$, where $\pi/2 \geq \theta \geq 0$ is the angle between the wavevector $\mathbf{k}_{1,2}$ and the x -axis. A schematic is given in FIG. 4. The electric fields of the KD lasers are modified from Eq. (40) to be

$$\mathbf{E}_{1,2}(x, t) = E_{1,2} \exp(-t^2/\tau_{\text{KD}}^2) \cos(-\mathbf{k}_{1,2} \cdot \mathbf{r} \pm \omega_{1,2} t) \vec{e}_z, \quad (53)$$

where $\mathbf{r} = (x, y, z)$ is the 3D position operator of the particle. Because the interaction involve both the x - and y -oscillators, the general solution to the particle's wavefunction is modified from Eq. (52) to be

$$|\psi\rangle(t) = |0\rangle_z e^{-i\Omega_z t/2} \left(\sum_{m=0}^{\infty} \sum_{n=0}^{\infty} C_{m,n}(t) e^{-i(\Omega_x^{(m)} + \Omega_y^{(n)})t} |m, n\rangle \right), \quad (54)$$

where $|m, n\rangle \equiv |m\rangle_x |n\rangle_y$, $\Omega_x^{(m)} \equiv \Omega_x(m + 1/2)$, and $\Omega_y^{(n)} \equiv \Omega_y(n + 1/2)$. The Schrödinger equation for $C_{m,n}(t)$ is

$$i\hbar \frac{dC_{m',n'}(t)}{dt} = \sum_{m=0}^{\infty} \sum_{n=0}^{\infty} \langle m', n' | \hat{H}_{int} | m, n \rangle C_{m,n}(t) e^{i(\Omega_x^{(m')} - \Omega_x^{(m)})t} e^{i(\Omega_y^{(n')} - \Omega_y^{(n)})t}. \quad (55)$$

Using Eq. (53), the interaction Hamiltonian in Eq. (49) is modified to be

$$\begin{aligned} \hat{H}_{int} = & -\frac{\alpha}{2} \exp(-2t^2/\tau_{\text{KD}}^2) [E_1^2 \cos^2(\mathbf{k}_1 \cdot \mathbf{r} - \omega_1 t) + E_2^2 \cos^2(\mathbf{k}_2 \cdot \mathbf{r} + \omega_2 t)] \\ & -\frac{\alpha}{2} E_1 E_2 \exp(-2t^2/\tau_{\text{KD}}^2) [\cos((\mathbf{k}_1 + \mathbf{k}_2) \cdot \mathbf{r} - (\omega_1 - \omega_2)t) + \cos((\mathbf{k}_1 - \mathbf{k}_2) \cdot \mathbf{r} - (\omega_1 + \omega_2)t)]. \end{aligned} \quad (56)$$

Assuming $\omega_{1,2}$ to be many orders of magnitude higher than the trap frequencies $\Omega_{x,y,z}$, only the $\omega_1 - \omega_2$ term in Eq. (56) can resonantly excite the harmonic oscillator. Therefore, Eq. (56) can be simplified as

$$\begin{aligned} \hat{H}_{int} = & -\frac{\alpha}{4} E_1 E_2 \exp(-2t^2/\tau_{\text{KD}}^2) \cos((\mathbf{k}_1 + \mathbf{k}_2) \cdot \mathbf{r}) \left(e^{i(\omega_1 - \omega_2)t} + e^{-i(\omega_1 - \omega_2)t} \right) \\ & + i\frac{\alpha}{4} E_1 E_2 \exp(-2t^2/\tau_{\text{KD}}^2) \sin((\mathbf{k}_1 + \mathbf{k}_2) \cdot \mathbf{r}) \left(e^{i(\omega_1 - \omega_2)t} - e^{-i(\omega_1 - \omega_2)t} \right), \end{aligned} \quad (57)$$

where $\cos((\omega_1 - \omega_2)t)$ and $\sin((\omega_1 - \omega_2)t)$ are expanded. The transition matrix element in Eq. (55) is thus

$$\langle m', n' | \hat{H}_{int} | m, n \rangle = f_{\alpha}(t) \langle m', n' | \cos((\mathbf{k}_1 + \mathbf{k}_2) \cdot \mathbf{r}) | m, n \rangle + h_{\alpha}(t) \langle m', n' | \sin((\mathbf{k}_1 + \mathbf{k}_2) \cdot \mathbf{r}) | m, n \rangle, \quad (58)$$

where

$$\begin{aligned} f_{\alpha}(t) & \equiv -(\alpha/2) E_1 E_2 \exp(-2t^2/\tau_{\text{KD}}^2) \cos((\omega_1 - \omega_2)t), \\ h_{\alpha}(t) & \equiv -(\alpha/2) E_1 E_2 \exp(-2t^2/\tau_{\text{KD}}^2) \sin((\omega_1 - \omega_2)t). \end{aligned} \quad (59)$$

Using Eq. (24), we can evaluate the matrix element

$$\langle m', n' | e^{i(\mathbf{k}_1 + \mathbf{k}_2) \cdot \mathbf{r}} | m, n \rangle = \int_{-\infty}^{\infty} dk_x \psi_{m'}^*(k_x) \psi_m(k_x - (k_1 + k_2)_x) \int_{-\infty}^{\infty} dk_y \phi_{n'}^*(k_y) \phi_n(k_y - (k_1 + k_2)_y), \quad (60)$$

where $\psi_n(k)$ and $\phi_n(k)$ are the eigen-wavefunctions of the x - and y -oscillators in the momentum space, and $(k_1 + k_2)_{x,y} \equiv (\mathbf{k}_1 + \mathbf{k}_2) \cdot \hat{\epsilon}_{x,y}$ are the projection of $\mathbf{k}_1 + \mathbf{k}_2$ along the x - and y -axes. Using Eq. (60), we transform Eq. (58) into

$$\begin{aligned} \langle m', n' | \hat{H}_{int} | m, n \rangle = & \pi \left[f_{\alpha}(t) \left(1 + (-1)^{m'+m+n'+n} \right) - i h_{\alpha}(t) \left(1 - (-1)^{m'+m+n'+n} \right) \right] \\ & \times \int_{-\infty}^{\infty} dk_x \psi_{m'}^*(k_x) \psi_m(k_x - (k_1 + k_2)_x) \int_{-\infty}^{\infty} dk_y \phi_{n'}^*(k_y) \phi_n(k_y - (k_1 + k_2)_y), \end{aligned} \quad (61)$$

which is a generalization of Eq. (26). With Eqs. (55) and (61), we can summarize the conditions for resonant excitation in terms of energy-momentum conservation,

$$\begin{cases} \omega_1 - \omega_2 = n_x \Omega_x + n_y \Omega_y \\ (k_1 + k_2)_x = (n_x + \delta_{px}) k_{x0} \\ (k_1 + k_2)_y = (n_y + \delta_{py}) k_{y0}, \end{cases} \quad (62)$$

where $n_{x,y}$ are positive integers, $k_{x0} = \sqrt{M\Omega_x/2\hbar}$, $k_{y0} = \sqrt{M\Omega_y/2\hbar}$, and $\delta_{px,py}$ are the momentum detuning for the x - and the y -oscillator respectively. The central KD laser frequency ω_{KD} and the laser propagation angle θ can be obtained from Eq. (62),

$$\begin{aligned} \omega_{\text{KD}} & = \frac{c}{2} \sqrt{(n_x + \delta_{px})^2 k_{x0}^2 + (n_y + \delta_{py})^2 k_{y0}^2} \\ \theta & = \tan^{-1} \left(\frac{n_y + \delta_{py}}{n_x + \delta_{px}} \sqrt{\frac{\Omega_y}{\Omega_x}} \right), \end{aligned} \quad (63)$$

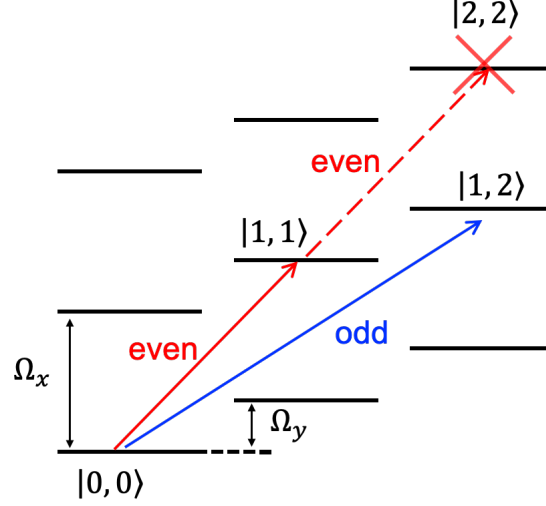


FIG. 5. (color online) A partial level scheme of a 3D harmonic oscillator that undergoes even or odd transitions under inelastic Kapitza-Dirac scattering.

so the KD laser frequencies are $\omega_{1,2} = \omega_{\text{KD}} \pm (n_x \Omega_x + n_y \Omega_y)/2$. We can see from Eqs. (61) and (62) that the joint parity change of the oscillator determines the symmetry of the transition, i.e. $(-1)^{m'+m+n'+n} = (-1)^{n_x+n_y}$. If n_x and n_y are both even or odd, then the transition is even and it involves only the $\cos((\mathbf{k}_1 + \mathbf{k}_2) \cdot \mathbf{r})$ term in Eq. (57). Otherwise, the transition is odd. An example is provided in FIG. 5. Using Eq. (30), we can evaluate Eq. (60) in terms of the generalized Laguerre polynomials,

$$\begin{aligned} \langle m', n' | e^{i(\mathbf{k}_1 + \mathbf{k}_2) \cdot \mathbf{r}} | m, n \rangle &= \langle m' | e^{i(k_1 + k_2)_x x} | m \rangle \langle n' | e^{i(k_1 + k_2)_y y} | n \rangle \\ &= \left(\sqrt{\frac{m!}{m'}} (i\eta_x)^{m'-m} e^{-\eta_x^2/2} L_m^{(m'-m)}(\eta_x^2) \right) \left(\sqrt{\frac{n!}{n'}} (i\eta_y)^{n'-n} e^{-\eta_y^2/2} L_n^{(n'-n)}(\eta_y^2) \right) \end{aligned} \quad (64)$$

for $m' > m$ and $n' > n$. Note that the Lamb-Dicke parameters here are $\eta_x = (n_x + \delta_{px})/2$ and $\eta_y = (n_y + \delta_{py})/2$. Assuming $m' = m + n_x$ and $n' = n + n_y$, the matrix element in Eq. (58) have the analytic forms

$$\begin{aligned} \langle m + n_x, n + n_y | \cos((\mathbf{k}_1 + \mathbf{k}_2) \cdot \mathbf{r}) | m, n \rangle &= \frac{1}{2} (1 + (-1)^{n_x+n_y}) (i)^{n_x+n_y} F_{m,n}^{(n_x,n_y)}(\eta_x, \eta_y) \\ \langle m + n_x, n + n_y | \sin((\mathbf{k}_1 + \mathbf{k}_2) \cdot \mathbf{r}) | m, n \rangle &= \frac{1}{2i} (1 - (-1)^{n_x+n_y}) (i)^{n_x+n_y} F_{m,n}^{(n_x,n_y)}(\eta_x, \eta_y), \end{aligned} \quad (65)$$

where

$$F_{m,n}^{(n_x,n_y)}(\eta_x, \eta_y) \equiv \sqrt{\frac{m!}{(m+n_x)!}} \sqrt{\frac{n!}{(n+n_y)!}} (\eta_x)^{n_x} (\eta_y)^{n_y} e^{-(\eta_x^2 + \eta_y^2)/2} L_m^{(n_x)}(\eta_x^2) L_n^{(n_y)}(\eta_y^2). \quad (66)$$

For $\omega_1 - \omega_2 = n_x \Omega_x + n_y \Omega_y$, the Schrödinger equation in Eq. (55) can be simplified to include only the resonant terms,

$$\begin{aligned} i\hbar \frac{dC_{m,n}(t)}{dt} &= \langle m, n | \hat{H}_{int} | m - n_x, n - n_y \rangle C_{m-n_x, n-n_y}(t) e^{i(n_x \Omega_x + n_y \Omega_y)t} \\ &\quad + \langle m, n | \hat{H}_{int} | m + n_x, n + n_y \rangle C_{m+n_x, n+n_y}(t) e^{-i(n_x \Omega_x + n_y \Omega_y)t}. \end{aligned} \quad (67)$$

In the case of even transitions $n_x + n_y = 2k$, where k is a positive integer, the matrix element in Eq. (67) can be evaluated from Eq. (65),

$$\langle m + n_x, n + n_y | \hat{H}_{int} | m, n \rangle = f_\alpha(t) \langle m + n_x, n + n_y | \cos((\mathbf{k}_1 + \mathbf{k}_2) \cdot \mathbf{r}) | m, n \rangle = f_\alpha(t) (-1)^k F_{m,n}^{(n_x,n_y)}(\eta_x, \eta_y). \quad (68)$$

Similarly, in odd transitions $n_x + n_y = 2k + 1$, the matrix element in Eq. (67) is

$$\langle m + n_x, n + n_y | \hat{H}_{int} | m, n \rangle = h_\alpha(t) \langle m + n_x, n + n_y | \sin((\mathbf{k}_1 + \mathbf{k}_2) \cdot \mathbf{r}) | m, n \rangle = h_\alpha(t) (-1)^k F_{m,n}^{(n_x, n_y)}(\eta_x, \eta_y). \quad (69)$$

Let us examine the two examples of even and odd transitions in FIG. 5. For the even transition $(n_x, n_y) = (1, 1)$, Eq. (68) becomes

$$\langle m + 1, n + 1 | \hat{H}_{int} | m, n \rangle = f_\alpha(t) g_{m,n}(\eta_x, \eta_y), \quad (70)$$

where

$$g_{m,n}(\eta_x, \eta_y) \equiv -F_{m,n}^{(1,1)}(\eta_x, \eta_y) = -\sqrt{\frac{m!}{(m+1)!}} \sqrt{\frac{n!}{(n+1)!}} (\eta_x \eta_y) e^{-(\eta_x^2 + \eta_y^2)/2} L_m^{(1)}(\eta_x^2) L_n^{(1)}(\eta_y^2). \quad (71)$$

The corresponding Schrödinger equation can be derived from Eq. (67),

$$i\hbar \frac{dC_{m,n}(t)}{dt} = f_\alpha(t) \left(g_{m-1,n-1}(\eta_x, \eta_y) C_{m-1,n-1}(t) e^{i(\Omega_x + \Omega_y)t} + g_{m,n}(\eta_x, \eta_y) C_{m+1,n+1}(t) e^{-i(\Omega_x + \Omega_y)t} \right). \quad (72)$$

For the odd transition $(n_x, n_y) = (1, 2)$, Eq. (69) becomes

$$\langle m + 1, n + 2 | \hat{H}_{int} | m, n \rangle = h_\alpha(t) \xi_{m,n}(\eta_x, \eta_y), \quad (73)$$

where

$$\xi_{m,n}(\eta_x, \eta_y) \equiv -F_{m,n}^{(1,2)}(\eta_x, \eta_y) = -\sqrt{\frac{m!}{(m+1)!}} \sqrt{\frac{n!}{(n+2)!}} (\eta_x \eta_y^2) e^{-(\eta_x^2 + \eta_y^2)/2} L_m^{(1)}(\eta_x^2) L_n^{(2)}(\eta_y^2), \quad (74)$$

and the corresponding Schrödinger equation is

$$i\hbar \frac{dC_{m,n}(t)}{dt} = h_\alpha(t) \left(\xi_{m-1,n-2}(\eta_x, \eta_y) C_{m-1,n-2}(t) e^{i(\Omega_x + 2\Omega_y)t} + \xi_{m,n}(\eta_x, \eta_y) C_{m+1,n+2}(t) e^{-i(\Omega_x + 2\Omega_y)t} \right). \quad (75)$$

From Eqs. (71) and (74), we see that the sequential transition can be fully stopped at certain values of momentum detunings, δ_{px} or δ_{py} . Therefore, KD blockade also works for 2D and 3D harmonic oscillators. Additionally, as the transition of one oscillator is suppressed, the transition of other oscillators stops too. Thus one set of laser parameters $(\omega_1, \omega_2, \theta)$ in Eq. (62) chosen for either δ_{px} or δ_{py} is sufficient for stopping transitions for both x - and y -oscillators. An entangled state $|\psi\rangle = (|0, 0\rangle + |1, 1\rangle)/\sqrt{2}$ between the x - and y -oscillators can be prepared by suppressing the transition $|1, 1\rangle \rightarrow |2, 2\rangle$ as shown in FIG. 5. Complex entangled states such as a 2-component cat state entangling with a 3-component cat state (see FIG. 4(d) and FIG. 5 in the main text) can be prepared by using the odd transition $(n_x, n_y) = (2, 3)$ and placing the blockade on the transition $|12, 18\rangle \rightarrow |14, 21\rangle$. Combination with a second pair of KD lasers along the y -axis allows preparation of entangled states between cat states and single eigenstates, $|\psi\rangle = ((|\alpha\rangle_x + |-\alpha\rangle_x)|0\rangle_y + (|\alpha\rangle_x - |-\alpha\rangle_x)|1\rangle_y)/2$, which make it possible to emulate a cavity-QED system with electrons, complex molecules, or dielectric nanoparticles.

II. Wigner function and wave function in the discrete limit

Given a wavefunction $\psi(x)$ in the configuration space, the Wigner function is [4]

$$W(q, p) = \frac{1}{2\pi\hbar} \int_{-\infty}^{\infty} \psi^* \left(q - \frac{x}{2} \right) \psi \left(q + \frac{x}{2} \right) e^{ipx/\hbar} dx, \quad (76)$$

where q and p are position and momentum respectively. Defining $k \equiv p/\hbar$ and $f_q(x) \equiv \psi^*(q - x/2) \psi(q + x/2)$, we can rewrite Eq. (76) as a Fourier transform of $f_q(x)$,

$$W(q, k) = \frac{1}{\hbar} \left(\frac{1}{2\pi} \int_{-\infty}^{\infty} dx f_q(x) e^{ikx} \right). \quad (77)$$

As (x, k) is a conjugated pair in Fourier transform, the integral can be discretized using the relation

$$\frac{1}{2\pi} \int dx \leftrightarrow \frac{1}{L_k} \sum_n \Delta n, \quad (78)$$

where $\Delta n = 1$, and the discreteness of x implies a finite size of the one-dimensional k -space $L_k = 2\pi/\Delta x$ with $\Delta x = x_{n+1} - x_n$. Using Eq. (78), we can transform Eq. (77) into

$$W(q, k) = \frac{1}{\hbar L_k} \sum_n f_q(x_n) e^{ikx_n}. \quad (79)$$

A change of variable gives the discretized form of the Wigner function in Eq. (76),

$$W(q, p) = \frac{\Delta x}{2\pi} \sum_n \psi^*(q - x_n/2) \psi(q + x_n/2) e^{ipx_n/\hbar}. \quad (80)$$

The Wigner functions presented in FIG. 4 and FIG. 5 of the main text are computed through Eq. (80). Additionally, we note that the probability distributions $|\psi(x)|^2$ and $|\varphi(p)|^2$ in the position and momentum space can be obtained as marginals of the Wigner function,

$$\begin{aligned} |\psi(x)|^2 &= \int_{-\infty}^{\infty} dp W(x, p) \leftrightarrow |\psi(x)|^2 = \frac{2\pi\hbar}{L_x} \sum_n W(x, p_n), \\ |\varphi(p)|^2 &= \int_{-\infty}^{\infty} dx W(x, p) \leftrightarrow |\varphi(p)|^2 = \frac{2\pi\hbar}{L_p} \sum_n W(x_n, p), \end{aligned} \quad (81)$$

where $L_p = \hbar L_k$.

In our numerical simulation of inelastic KD scattering, the time-dependent Schrödinger equations in Eq. (34) and Eq. (36) are solved for a N -state harmonic oscillator. The real and imaginary part of the Schrödinger equation are separated, so there are $2N$ real-number differential equations to be solved simultaneously. We employ the adaptive 5th order Cash-Karp Runge-Kutta method as the equation solver in our FORTRAN code [6]. The oscillator is assumed to be in the ground state initially. The integration time is 5 times longer than the $1/e$ pulse duration of the KD lasers. The integration stepsize is $1/100$ of the natural period $2\pi/\Omega_0$. The most computationally intense simulation is for a nanoparticle oscillator with $N = 10500$ eigenstates (see FIG. 6(c) in the main text). The simulation took 400 GB memory and 83 hours of computation time on a single core of a supercomputer (Rhino, Holland Computing Center). The data size is 0.5 GB. Once we obtain the probability amplitude $C_n(t)$ for each eigenstate, we compute the oscillator's wavefunction using MATLAB, and the wavefunction is subsequently used for computing the Wigner function in Eq. (80). We note that for states $n > 170$ the value of the normalization factor $\sqrt{1/2^n n!}$ in the analytical formula of the oscillator eigen-wavefunction is too large for the computer to compute. To circumvent this problem, we solve the eigen-wavefunction numerically using the time-independent Schrödinger equation in the range of $0 \leq x \leq x_t$, where $x_t = \sqrt{(n+1/2)2\hbar/M\Omega_0}$ is the turning point. In the tunneling regime $x \geq x_t$, we patch an ansatz function to the eigen-wavefunction

$$\phi(x \geq x_t) = \phi(x_t) \exp \left[\frac{(x - x_t)\phi'(x_t)}{\phi(x_t)} \right] \exp \left[-\frac{(x - x_t)^2}{2x_0^2} \right], \quad (82)$$

where $\phi'(x) \equiv d\phi(x)/dx$ and $x_0 = \sqrt{\hbar/2M\Omega_0}$. The eigen-wavefunction in the range of $x < 0$ is obtained through symmetry $\phi(x < 0) = (-1)^n \phi(-x)$, where n is the quantum number of the eigenstate. The numerically solved eigen-wavefunctions are in very good agreement with the analytic formula. The data size of the nanoparticle oscillator eigen-wavefunctions is 50 GB.

III. Evaluation of the maximum spatial and momentum separation of a cat state

We first consider a coherent state $|\alpha\rangle(t)$ oscillating back and forth in a harmonic potential. The Hamiltonian for a harmonic oscillator with a mass M and a natural frequency Ω_0 is

$$\hat{H} = \frac{\hat{p}^2}{2M} + \frac{1}{2}M\Omega_0^2\hat{x}^2 = \frac{(\hat{p} - p_c)^2 + 2(\hat{p} - p_c)p_c + p_c^2}{2M} + \frac{1}{2}M\Omega_0^2[(\hat{x} - x_c)^2 + 2(\hat{x} - x_c)x_c + x_c^2], \quad (83)$$

where $p_c = \langle \hat{p} \rangle(t)$ and $x_c = \langle \hat{x} \rangle(t)$ are the momentum and the position expectation values of the wavepacket at time t . The energy expectation value is

$$\langle \hat{H} \rangle(t) = \frac{\langle (\hat{p} - p_c)^2 \rangle + 2\langle \hat{p} - p_c \rangle p_c + p_c^2}{2M} + \frac{1}{2}M\Omega_0^2 [\langle (\hat{x} - x_c)^2 \rangle + 2\langle \hat{x} - x_c \rangle x_c + x_c^2]. \quad (84)$$

Because the Gaussian probability distribution of the coherent state is symmetric with respect to its average momentum and position, p_c and x_c , we have $\langle \hat{p} - p_c \rangle = 0$ and $\langle \hat{x} - x_c \rangle = 0$, and Eq. (84) is simplified to

$$\langle \hat{H} \rangle(t) = \left(\frac{\langle (\hat{p} - p_c)^2 \rangle}{2M} + \frac{1}{2}M\Omega_0^2 \langle (\hat{x} - x_c)^2 \rangle \right) + \left(\frac{p_c^2}{2M} + \frac{1}{2}M\Omega_0^2 x_c^2 \right). \quad (85)$$

The terms in the first parenthesis are the kinetic and potential energies associated with the spread of the wavepacket, $\sigma_x^2 = \langle (\hat{x} - x_c)^2 \rangle$ and $\sigma_p^2 = \langle (\hat{p} - p_c)^2 \rangle$. The terms in the second parenthesis give the kinetic and potential energies associated with the average momentum and position of the wavepacket, which evolve as those of a classical harmonic oscillator according to the Ehrenfest theorem. Since the coherent state have the same Gaussian probability distribution as the ground state, the terms in the first parenthesis are equal to $\hbar\Omega_0/2$, and Eq. (85) is further simplified as

$$\langle \hat{H} \rangle(t) = \frac{\hbar\Omega_0}{2} + \left(\frac{p_c^2}{2M} + \frac{1}{2}M\Omega_0^2 x_c^2 \right). \quad (86)$$

Now, we consider a cat state $|\psi\rangle_{cat}(t) = (|\alpha\rangle(t) + |-\alpha\rangle(t))/\sqrt{2}$ in the harmonic potential. We assume that the width of the two wavepackets $|\alpha\rangle$ and $|-\alpha\rangle$ are smaller than the maximum spatial separation Δx_{cat} between the peaks of the two wavepackets. At the turning points, i.e. $x_c = \Delta x_{cat}/2$, the energy expectation values associated with each wavepackets can be calculated using Eq. (86),

$$\langle E \rangle_{1,2} = \frac{\hbar\Omega_0}{2} + \frac{1}{2}M\Omega_0^2 \left(\frac{\Delta x_{cat}}{2} \right)^2. \quad (87)$$

Meanwhile, the energy expectation value of the cat state can be calculated from the population distribution,

$$\langle E \rangle_{cat} = \hbar\Omega_0 \left(\langle n \rangle + \frac{1}{2} \right). \quad (88)$$

Assuming sufficiently large $|\alpha|$, i.e. well-separated wavepackets, we have $\langle -\alpha | \alpha \rangle = 0$, so $\langle E \rangle_{cat}$ can be related to $\langle E \rangle_{1,2}$ by

$$\langle E \rangle_{cat} = \frac{1}{2} \left(\langle \alpha | \hat{H} | \alpha \rangle + \langle -\alpha | \hat{H} | -\alpha \rangle \right) = \frac{1}{2} (\langle E \rangle_1 + \langle E \rangle_2). \quad (89)$$

Substituting Eqs. (87) and (88) to Eq. (89), we obtain a relation between the maximum spatial separation Δx_{cat} and the quantum number at the peak of the population distribution $n_{max} \equiv \langle n \rangle$,

$$\frac{\Delta x_{cat}}{x_0} = 4\sqrt{n_{max}}, \quad (90)$$

where $x_0 = \sqrt{\hbar/2M\Omega_0}$. Similarly, at the potential minimum, Eq. (86) becomes

$$\langle E \rangle_{1,2} = \frac{\hbar\Omega_0}{2} + \frac{1}{2M} \left(\frac{\Delta p_{cat}}{2} \right)^2. \quad (91)$$

Again, substituting Eqs. (88) and (91) to Eq. (89) we obtain a relation between the maximum momentum separation Δp_{cat} and n_{max} ,

$$\frac{\Delta p_{cat}}{\hbar k_0} = 4\sqrt{n_{max}}, \quad (92)$$

where $k_0 = \sqrt{M\Omega_0/2\hbar}$.

While the above analysis assumes a cat state made of two coherent state wavepackets, the result can be used for other cat states as an approximation if the component wavepackets are Gaussian-like and the width of the population

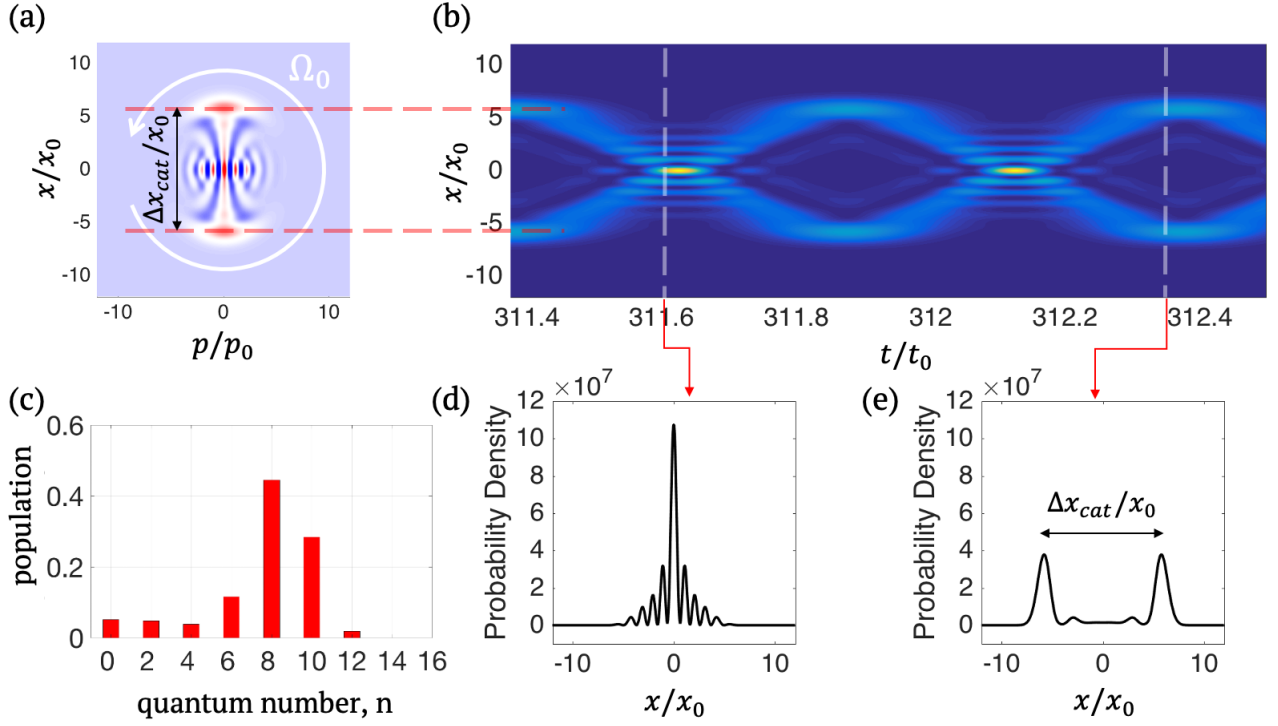


FIG. 6. (color online) Free oscillation of an amplitude-squeezed Schrödinger cat state in a harmonic potential. (a) The Wigner function $W(x, p, t)$ of an amplitude-squeezed Schrödinger cat state rotates in the counter-clockwise direction as time evolves. Note that $p_0 \equiv \hbar k_0$ and $t_0 \equiv 2\pi/\Omega_0$. (b) The probability distribution as a function of time is given by the projection of the Wigner function along the x -axis, $P(x, t) = \int_{-\infty}^{\infty} dp W(x, p, t)$. The two branches of the probability trace show that the two wavepackets of the cat state oscillate back and forth in the harmonic potential. (c) The population distribution of the amplitude-squeezed Schrödinger cat state peaks at $n_{\max} = 8$. (d) The probability distribution shows interference fringes as the two wavepackets cross the potential minimum. (e) As the two wavepackets reach the turning points, the probability distribution shows two distinct peaks separated by $\Delta x_{\text{cat}} \approx 11x_0$.

distribution is sub-Poissonian, i.e. amplitude squeezed. Assuming $n_{\max} \gg 1$, the energy expectation value of such cat states can be estimated as

$$\langle E \rangle_{\text{cat}} \approx n_{\max} \hbar \Omega_0, \quad (93)$$

because the population distribution is narrowly centered around n_{\max} with a sub-Poissonian width. Also, for wavepacket separation much larger than the squeezed widths $\Delta x_{\text{cat}} \gg \sigma_x$ and $\Delta p_{\text{cat}} \gg \sigma_p$, Eq. (85) can be approximated as

$$\langle E \rangle_{1,2} \approx \frac{1}{2} M \Omega_0^2 x_c^2 = \frac{1}{2} M \Omega_0^2 \left(\frac{\Delta x_{\text{cat}}}{2} \right)^2 \quad (94)$$

at the turning points, and

$$\langle E \rangle_{1,2} \approx \frac{p_c^2}{2M} = \frac{1}{2M} \left(\frac{\Delta p_{\text{cat}}}{2} \right)^2 \quad (95)$$

at the potential minimum. Therefore, using Eqs. (93), (94), and (95) we again obtain the relations between Δx_{cat} , Δp_{cat} , and n_{\max} ,

$$\frac{\Delta x_{\text{cat}}}{x_0} = \frac{\Delta p_{\text{cat}}}{\hbar k_0} \approx 4\sqrt{n_{\max}}. \quad (96)$$

An example is given in FIG. 6, which is an amplitude-squeezed Schrödinger cat state prepared through our simulation of inelastic KD scattering. In this example, we see that $n_{\max} = 8$ and $\Delta x_{\text{cat}}/x_0 = \Delta p_{\text{cat}}/\hbar k_0 \approx 11$, which is consistent

with FIG. 6(a) and (e). In FIG. 6 of the main text, we show three very large cat states whose population distributions peak at $n_{\max} = 648$ (electron), 7822 (molecule) and 10280 (nanoparticle). The full width of the distributions are 6 (electron), 8 (molecule), and 8 (nanoparticle), which are well below the full Poissonian width $2\sigma_p = 2\sqrt{n_{\max}}$. Therefore, the estimated maximum separations are $\Delta x_{\text{cat}}/x_0 = \Delta p_{\text{cat}}/\hbar k_0 \approx 101$ (electron), 353 (molecule), 405 (nanoparticle), which are in good agreement with the probability distributions shown in FIG. 6 of the main text.

IV. Determination of the highest eigenstate available for excitation

(a) Pondermotive trap for electrons

We consider an electron in the pondermotive trap described in Eq. (9), $U_p(x) = U_0 \cos^2(k_{\text{TL}}x)$. Expanding around the potential minimum $x_m = \lambda_{\text{TL}}/4$ gives

$$U_p(x) \approx U_0 k_{\text{TL}}^2 \left[x^2 - \frac{1}{3} k_{\text{TL}}^2 x^4 \right], \quad (97)$$

where x is repurposed as the displacement from the minimum. The harmonic approximation, $U_p(x) \approx U_0 k_{\text{TL}}^2 x^2$, is valid when $x \ll x_{\max}$, where $x_{\max} = \sqrt{3}/k_{\text{TL}}$. As the iterative excitation cannot continue effectively in the anharmonic regime, there is a limit to the maximum spatial separation of cat states, i.e. $\Delta x_{\text{cat}} \ll 2x_{\max}$. Using Eq. (96), we identify the upper bound for n_{\max} as,

$$n_{\max} \ll \frac{3}{16\pi^2} \left(\frac{\lambda_{\text{TL}}}{x_0} \right)^2. \quad (98)$$

(b) Dipole trap for polarizable particles

We consider a polarizable neutral particle in the dipole trap described in Eq. (45),

$$U_d(x) = \frac{-\alpha I_{\text{TL}}}{2\epsilon_0 c} \exp(-8x^2/W_{x\text{-TL}}^2), \quad (99)$$

where $W_{x\text{-TL}}$ is the $1/e$ beam diameter along the x -axis. Expanding around potential minimum $x_m = 0$ gives

$$U_d(x) \approx \frac{4\alpha I_{\text{TL}}}{\epsilon_0 c W_{x\text{-TL}}^2} \left(x^2 - 4 \frac{x^4}{W_{x\text{-TL}}^2} \right), \quad (100)$$

where a constant in the expansion is dropped. The harmonic approximation,

$$U_d(x, 0) \approx \frac{4\alpha I_{\text{TL}}}{\epsilon_0 c W_{x\text{-TL}}^2} x^2, \quad (101)$$

is valid when $x \ll x_{\max}$, where $x_{\max} = W_{x\text{-TL}}/2$. As before, $\Delta x_{\text{cat}} \ll 2x_{\max}$. Using Eq. (96), the upper bound for n_{\max} is

$$n_{\max} \ll \frac{1}{16} \left(\frac{W_{x\text{-TL}}}{x_0} \right)^2. \quad (102)$$

-
- [1] W. C. Huang and H. Batelaan, *Atoms* **7**, 42 (2019).
 - [2] K. E. Cahill and R. J. Glauber, *Phys. Rev.* **177**, 1857 (1969).
 - [3] D. J. Wineland, C. Monroe, W. M. Itano, B. E. King, D. Leibfried, D. M. Meekhof, C. Myatt, and C. Wood, *Fortschr. Phys.* **46**, 363 (1998).
 - [4] C. C. Gerry2005 and P. L. Knight, *Introductory Quantum Optics* (Cambridge University Press, New York) 2005.
 - [5] H. Batelaan, *Contemp. Phys.* **41**, 369 (2000).
 - [6] W. H. Press, S. A. Teukolsky, W. T. Vetterling, and B. P. Flannery, *Numerical Recipes in Fortran 77: The Art of Scientific Computing*, Cambridge University Press, 2nd edition, 1996.